of all such intensities to be used in modelling. Only 37 independent peaks in the same plane as the diffuse scattering were used in this preliminary work. The RMCX algorithm was essentially unchanged, but two goodness-of-fit parameters were calculated, one for Bragg and one for diffuse scattering, and these were then added with a scaling factor β, such that

$$\chi^2_{\text{total}} = \chi^2_{\text{diffuse}} + \beta R_w. \qquad (A1)$$

χ^2_{diffuse} is given by equation (4) of the main text, whilst the weighted R factor, R_w, used for Bragg scattering is defined by

$$R_w = \left\{ \sum_m \left[I_E(\mathbf{Q}_m) - I_C(\mathbf{Q}_m) \right]^2 / \sigma_E(\mathbf{Q}_m)^2 \right\} \times \left[\sum_m I_E(\mathbf{Q}_m)^2 / \sigma_E(\mathbf{Q}_m)^2 \right]^{-1}. \qquad (A2)$$

In this expression, $I_E(\mathbf{Q}_m)$ is the normalized experimental integrated intensity of the mth Bragg peak and $I_C(\mathbf{Q}_m)$ its calculated counterpart. $\sigma_E(\mathbf{Q}_m)$ is the corresponding experimental error. To fit both types of data well it was necessary initially to make the scaling factor β very large, so that a very good fit to the Bragg scattering was obtained (R_w of the order 10^{-4}). β was then decreased in stages, with convergence achieved at each stage. It is hence a very computationally expensive procedure.

Fig. 6 shows the experimental diffuse scattering from SXD for lead at 293 K, together with the RMCX fit. The agreement is good considering the poor statistics and large systematic errors in the data. (The systematic errors arose largely because the measurement was made with a small position-sensitive detector and the exact sample angle for each detector position is not known so that the joining of different segments of data could not be done with sufficient accuracy.) Good agreement was also obtained with the Bragg intensities, with a weighted R factor of 0.05, close to the 0.03 obtained by refinement of the Bragg peaks alone. The mean square displacements in the two cases were also in reasonable agreement, with a value of 0.029 (3) Å^2 in the present study and 0.024 (1) Å^2 from analysis solely of the Bragg intensities. This gives encouragement that Bragg and diffuse scattering can be fitted simultaneously. Work on optimizing the algorithm is continuing.

References

BERNAL, J. D. & FOWLER, R. H. (1993). *J. Chem. Phys.* **1**, 515–519.
BRÜNGER, A. T., KURIYAN, J. & KARPLUS, M. (1987). *Science*, **235**, 458–460.
FLORIANO, M. A., KLUG, D. D., WHALLEY, E., SVENSSON, E. C., SEARS, V. F. & HALLMAN, E. D. (1987). *Nature (London)*, **329**, 821–823.
HOWE, M. A., MCGREEVY, R. L. & HOWELLS, W. S. (1989). *J. Phys. Condens. Matter*, **1**, 3433–3451.
KUHS, W. F. & LEHMANN, M. S. (1986). *Water Sci. Rev.* **2**, 1–65.
KUHS, W. F. & LEHMANN, M. S. (1987). *J. Phys.* **48**(C1), 3–8.
LI, J. C., NIELD, V. M., ROSS, D. K., WHITWORTH, R. W., WILSON, C. C. & KEEN, D. A (1994). *Philos. Mag.* B**69**, 1173–1181.
LOVESEY, S. W. (1984). *Theory of Neutron Scattering from Condensed Matter*, Vol. I. pp. 29–30. Oxford Univ. Press.
MCGREEVY, R. L. & HOWE, M. A. (1992). *Ann. Rev. Mater. Sci.* **22**, 217–242.
MCGREEVY, R. L. & PUSZTAI, L. (1988). *Mol. Simul.* **1**, 359–367.
METROPOLIS, N., ROSENBLUTH, A. W., ROSENBLUTH, M. N., TELLER, A. H. & TELLER, E. J. (1953). *J. Chem. Phys.* **21**, 1087–1094.
NEWSAM, J. M., DEEM, M. W. & FREEMAN, C. M. (1992). *Natl Inst. Stand. Technol. Spec. Publ.* No. 846, pp. 80–91.
NIELD, V. M., HOWE, M. A. & MCGREEVY, R. L. (1991). *J. Phys. Condens. Matter*, **3**, 7519–7525.
NIELD, V M., KEEN, D. A., HAYES, W. & MCGREEVY, R. L. (1992). *J. Phys. Condens. Matter*, **4**, 6703–6714.
NIELD, V. M., KEEN, D. A., HAYES, W. & MCGREEVY, R. L. (1993). *Solid State Ion.* **66**, 247–258.
NIELD, V. M. & WHITWORTH, R. W. (1995). *J. Phys. Condens. Matter.* Submitted.
RÖTTGER, K., ENDRISS, A., IHRINGER, J., DOYLE, S. & KUHS, W. F. (1994). *Acta Cryst.* B**50**, 644–648.
WHALLEY, E. (1974). *Mol. Phys.* **28**, 1105–1108.
WLODAWER, A. & HENDRICKSON, W. A. (1982). *Acta Cryst.* A**38**, 239–247.

Acta Cryst. (1995). A**51**, 771–790

Diffraction by Disordered Polycrystalline Fibers

BY W. J. STROUD AND R. P. MILLANE*

Whistler Center for Carbohydrate Research, Purdue University, West Lafayette, Indiana 47907-1160, *USA*

(*Received* 9 *September* 1994; *accepted* 15 *February* 1995)

Abstract

X-ray diffraction patterns from some polycrystalline fibers show that the constituent microcrystallites are disordered. The relationship between the crystal structure and the diffracted intensities is then quite complicated and depends on the precise kind and degree of disorder present. The effects of disorder on diffracted intensities must be included in structure determinations using diffraction data from such specimens. Theory and algorithms are developed here that allow the full

* To whom all correspondence should be addressed.

diffraction pattern to be calculated for a disordered polycrystalline fiber made up of helical molecules. The model accommodates various kinds of disorder and includes the effects of finite crystallite size and cylindrical averaging of the diffracted intensities from a fiber. Simulations using these methods show how different kinds, or components, of disorder produce particular diffraction effects. General properties of disordered arrays of helical molecules and their effects on diffraction patterns are described. Implications for structure determination are discussed.

1. Introduction

X-ray fiber diffraction analysis is used to determine the molecular and crystal structures of polymers and rod-like macromolecular assemblies that can be prepared as oriented fibers or as rotationally disordered planar arrays (Arnott, 1980; Millane, 1988). The degree of order in these specimens varies greatly, as evidenced by the variety of diffraction patterns they give. In a *non-crystalline fiber*, the diffracting particles are oriented with their long axes approximately parallel but are randomly positioned and randomly rotated about these axes. The diffraction pattern is free from interparticle interference effects and shows continuous intensity, distributed on layer lines, that is equal to the cylindrical average of the intensity diffracted from a single molecule. In a *polycrystalline fiber*, the molecules form small well ordered crystallites that are randomly rotated about the long axes of the constituent molecules. The diffraction pattern consists of discrete Bragg reflections and is equivalent to the cylindrical projection of the diffraction pattern from a single crystal. It is, therefore, straightforward to calculate the intensity diffracted by non-crystalline and polycrystalline fiber specimens. Such a calculation is a necessary ingredient in structure determination. Diffraction data from polycrystalline specimens has been used to determine a wide range of polynucleotide, polysaccharide and synthetic polymer structures (Arnott, 1980; Millane, 1988). Data from non-crystalline specimens has also been used to determine the structures of some molecules (Namba & Stubbs, 1985; Millane, Chandrasekaran, Arnott & Dea, 1988).

It is not uncommon, however, for fibers to give diffraction patterns that display both sharp reflections and continuous intensity on layer lines (Miller & Parry, 1974; Arnott, 1980), indicating that the packing of the constituent molecules is neither ideally crystalline nor ideally non-crystalline. The sharp reflections are either confined to the center of the pattern and give way to continuous intensity at the periphery, as in the example shown in Fig. 1, or are dispersed across the pattern with intervening diffuse layer-line streaks. Fibers giving these kinds of pattern include those of C-DNA (Marvin, Spencer, Wilkins & Hamilton, 1961), the high-humidity α forms of synthetic polynucleotides (Arnott, Chandrasekaran, Millane & Park, 1986; Park, Arnott, Chandrasekaran, Millane & Campagnari, 1987), triple-stranded polynucleotides (Arnott & Bond, 1973), collagen (Fraser & MacRae, 1987), keratin (Fraser, MacRae, Parry & Suzuki, 1969), xanthan (Okuyama, Arnott, Moorhouse, Walkinshaw, Atkins & Wolf-Ullish, 1980), some polypeptides (Arnott, Dover & Elliot, 1967; Arnott & Dover, 1967; Inouye, Fraser & Kirschner, 1993) and ι-carrageenan (Arnott, Scott, Rees & McNab, 1974). A mixture of Bragg and continuous intensity in a diffraction pattern can result from a mixture of crystalline and non-crystalline material (Miller & Parry, 1974) but in many cases it results from imperfect, or disordered, crystalline packing of the molecules in a fiber. Diffraction patterns containing Bragg reflections at low resolution and continuous intensity at high resolution have been used to determine several polynucleotide structures (Arnott, Chandrasekaran, Millane & Park, 1986; Park, Arnott, Chandrasekaran, Millane & Campagnari, 1987) by co-refining molecular and crystal structures against the continuous and Bragg diffraction. Such an analysis is only approximately valid at best, since it ignores the effects of disorder on the diffracted intensities. Modeling disorder in polycrystalline fibers, and quantifying its effect on diffraction, is necessary for accurate structure determination using these kinds of patterns. Furthermore, identifying the kinds of disorder in a fiber may be important in its own right with regard to its relevance to the structure–function relationships of the molecules and the aggregates they form (Miller & Parry, 1974).

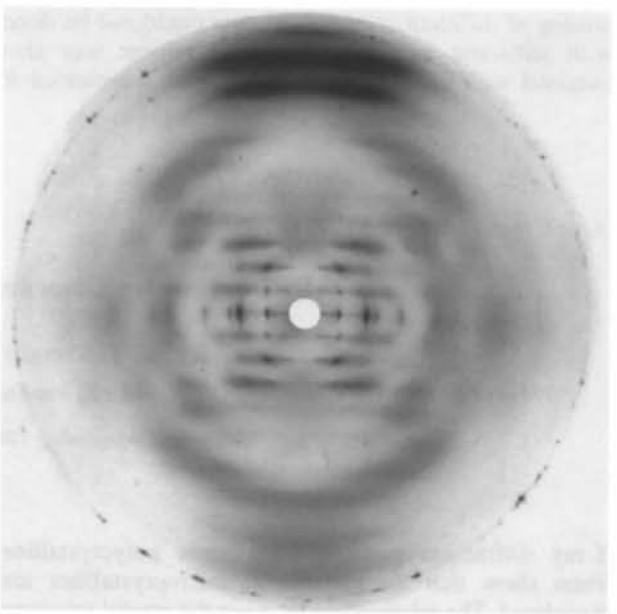

Fig. 1. Fiber diffraction pattern from poly(dA)·poly(rU) (Arnott, Chandrasekaran, Millane & Park, 1986).

The diffraction patterns we consider show little evidence of peak broadening with increasing resolution, indicating that the disorder is, to a good approximation, 'uncorrelated' (Hosemann & Bagchi, 1962; Welberry, 1985). This means that the distortions at one lattice site are independent of the distortions at other sites. The model we develop is therefore one of uncorrelated disorder (sometimes referred to as 'disorder of the first kind'). Several models of disorder in fibers incorporating rotations and axial translations of the molecules in each crystallite have appeared in the literature. Clark & Muus (1962) derive equations for the Bragg intensity diffracted from a fiber with this kind of disorder, for the case where only one Bessel order contributes to the intensity on each layer line. Tanaka & Naya (1969) develop the same model of disorder in more detail, deriving equations for both the Bragg and continuous intensity, while also considering the effects of random chain direction. Arnott (1980) does likewise but omits cylindrical averaging from the analysis. Each of these analyses is incomplete in some respect; none of them include the effects of lateral displacements of the molecules (which we show to be important) nor do they provide results that can be applied for computing the effects of disorder on diffraction patterns in detail. Vainshtein (1966, ch. V, equation 133) derives a general equation for diffraction from a fiber but does not complete its detailed development for the types of disorder considered here. His analysis of disorder is primarily concerned with the effects of ideal paracrystalline lattice distortions (Hosemann & Bagchi, 1962).

The advent of methods for accurately measuring continuous diffraction data (Fraser, MacRae, Miller & Rowlands, 1976; Makowski, 1978; Millane & Arnott, 1986) affords the possibility of a more detailed consideration of the effects of disorder in structure determination. Here, we extend earlier models of disordered polycrystalline fibers by including the lattice distortions that accompany other forms of disorder and derive equations that permit the complete distribution of intensity diffracted from model fibers to be calculated. Some aspects of our model have been described in a previous report (Millane & Stroud, 1991) but the analysis of the model presented here is considerably more detailed. The effects of the types of disorder generally thought to be present in fibers are examined in detail by calculation of diffraction patterns.

2. Preliminaries

2.1. *Diffraction from a helical molecule*

The complex amplitude, $F_l(R,\psi)$, diffracted by a molecule with u_v helix symmetry (u repeat units and v turns of the molecular helix in one c repeat) and infinite length, is restricted to the planes $Z = l/c$ of reciprocal space and is given by (Cochran, Crick & Vand, 1952; Klug, Crick & Wyckoff, 1958)

$$\begin{aligned} F_l(R,\psi) &= F(R,\psi,Z=l/c) \\ &= \sum_n G_{nl}(R)\exp[in(\psi+\pi/2)], \end{aligned} \quad (1)$$

where (R,ψ,Z) are cylindrical polar coordinates in reciprocal space. The *Fourier–Bessel structure factors*, $G_{nl}(R)$, are defined as

$$G_{nl}(R) = \sum_j f_j(\rho)J_n(2\pi r_j R)\exp[i(2\pi z_j l/c - n\varphi_j)], \quad (2)$$

where ρ is the length of the reciprocal-space position vector (R,ψ,Z), $J_n(x)$ is the nth-order Bessel function of the first kind, the sum over j is over all atoms in the repeat unit, and $f_j(\rho)$ is the scattering factor of the jth atom with cylindrical polar coordinates (r_j,φ_j,z_j). The summation in (1) is over all Bessel orders satisfying the helix selection rule

$$l = um + vn, \quad (3)$$

where m is any integer. For each layer-line index l, the selection rule has an infinite number of solutions n. However, the behavior of Bessel functions is such that for a molecule with maximum radius $r_{\max}$ only those $G_{nl}(R)$ for which

$$|n| \lesssim n_{\max} = 2\pi r_{\max} R + 2 \quad (4)$$

are significant at radius R (Crowther, DeRosier & Klug, 1970; Makowski, 1982).

As a result of cylindrical averaging, the layer-line intensities diffracted from an ideal non-crystalline fiber are given by (Franklin & Klug, 1955)

$$I_l(R) = (1/2\pi)\int_0^{2\pi} |F_l(R,\psi)|^2\,\mathrm{d}\psi = \sum_n |G_{nl}(R)|^2. \quad (5)$$

The layer-line intensities diffracted from a polycrystalline fiber consist of sharp Bragg reflections and are given by

$$I_l(R) = (1/2\pi)\int_0^{2\pi} I_{\text{crystallite}}(R,\psi,l/c)\,\mathrm{d}\psi, \quad (6)$$

where $I_{\text{crystallite}}(R,\psi,l/c)$ is the Bragg intensity diffracted from a representative crystallite.

2.2. *Disorder*

A review of the various models of diffraction by disordered systems (Welberry, 1985) shows that, regardless of the type of material for which they are specifically developed, they are founded on similar concepts and assumptions. It is generally assumed that materials that give diffraction patterns containing some sharp peaks are

crystalline on average but contain defects that interrupt the regularity of the crystal structure. These defects could be studied by directly modeling the interactions between the constituent units of a crystal, generating representative model crystals into which various defects have been introduced and calculating their diffraction patterns. However, results obtained by this approach depend critically on the accuracy of the interaction parameters used. In addition, the computational cost of generating ensembles of disordered crystallites is prohibitive in many cases. To date, this approach has been used to study disorder in polycrystalline fibers only on a very local scale (Rutledge & Suter, 1991). The approach we adopt for identifying and characterizing disorder in a specimen involves construction of statistical models of disordered crystallites and comparison of the resulting diffraction patterns with measured diffraction patterns. Disorder is described in terms of perturbations away from ideal three-dimensional crystalline order, and probability density functions characterizing these perturbations are defined. The average diffraction calculated over an ensemble of imperfect crystallites is then identified with the diffraction from a fiber. It is assumed that the statistics of the perturbations are *stationary*, *i.e.* invariant of position, a necessary assumption if the intensity diffracted from a crystal is to be calculated other than by a direct Fourier summation over every site of the crystal lattice.

It is convenient to regard disorder as having two related components, referred to here as *lattice disorder* and *substitution disorder*. Provided the crystal structure is not disrupted, it can be assumed that, on average, the molecules are located at the sites of a regular lattice. Lattice disorder consists only of deviations in the positions of the molecules from the average lattice. Disorder in the systems we are considering, however, also involves variations in the orientations of the molecules. This is not encompassed by lattice disorder but rather by substitution disorder. Substitution disorder consists of variations in the kinds of units at each lattice site or, since a single molecule in different orientations may be considered to be different molecules, variations in the orientation. Lattice disorder could also be considered as a component of substitution disorder but this is not generally done as the diffraction effects of the former are easier to describe than those of the latter.

Variations in the orientations of a molecule will generally affect the positions of neighboring molecules so that substitution disorder can generally be thought of as a source of lattice disorder. When disorder is confined to one dimension, as it is in the case of layered crystals (Hendricks & Teller, 1942; Wilson, 1942), or when the constituent units of a crystal are relatively simple, as they are in binary alloys (Cowley, 1968), the relationship between lattice distortion and substitution disorder can be specified. Otherwise, it is difficult to relate distortions of the lattice to variations in the orientations of the molecules, so that substitution disorder and lattice distortions must be treated as independent. This approach is adopted here.

3. Theory

The diffraction pattern from a polycrystalline fiber is dominated by the intensity diffracted from the crystalline domains, and is ideally confined to discrete layer lines. Intensity diffracted from amorphous material in the fiber contributes to a diffuse, approximately isotropic, background intensity that is generally modeled and subtracted from a diffraction pattern prior to the measurement of Bragg or continuous layer-line intensities (Millane & Arnott, 1985). For the purpose of calculating these intensities, a polycrystalline fiber can be modeled as a statistical ensemble of independent crystallites formed from the helical molecules. The crystallites are randomly positioned relative to each other and oriented so that their crystallographic c axes (chosen parallel to the helix axes of the molecules) are approximately parallel and randomly rotated about the c axis. The ensemble is then characterized by the lateral sizes and shapes of the crystallites and the statistics of the disorder within them.

We restrict our attention to specimens where the average crystalline structure has a monoclinic cell with one molecule per unit cell and with the c axis being the unique axis. This accommodates most polycrystalline fibers of biopolymers. In the absence of lattice disorder, the helix axes of the molecules intersect the lateral plane at the sites of a two-dimensional periodic lattice generated from the unit-cell vectors **a** and **b**. Lattice disorder is described here in terms of distortions of this lattice in three-dimensional space. The molecules are treated as rigid bodies, and substitution disorder as consisting of rotations about and translations along the helix axes and variations in the direction ('up' or 'down') of the molecules. The structural periodicity of the molecules in the axial direction remains, so that the diffracted intensity is confined to layer lines, as it is for the case of no disorder.

To derive expressions for the layer-line intensities diffracted from a fiber, we model the molecules in the crystallites as having infinite length and ignore the effects of disorientation. The resulting layer-line intensities can be corrected for these effects subsequently, as described in a later section. Without these corrections, the ensemble of crystallites representing the fiber diffracts layer-line intensities $I_l(R)$ given by

$$I_l(R) = \langle\langle\langle I(R, \psi, Z = l/c)\rangle_d\rangle_s\rangle_\psi, \qquad (7)$$

where $I(R, \psi, Z)$ is the intensity diffracted from a single crystallite, c is the axial repeat distance of the molecules, $\langle\ \rangle_d$ denotes averaging over all states of disorder, $\langle\ \rangle_s$ denotes averaging over all cross-sectional sizes and shapes of the crystallites in a plane perpendicular to the

fiber axis and $\langle\ \rangle_\psi$ denotes cylindrical averaging arising from the random rotations of the crystallites about their c axes. Equation (7) is the analog of equation (6) for a disordered fiber. Our goal is to evaluate the right-hand-side of (7) for a particular model of disorder.

3.1. *General formulation*

The molecules in a crystallite are displaced from the sites of the two-dimensional periodic lattice

$$\mathbf{r}_{jk} = j\mathbf{a} + k\mathbf{b} \tag{8}$$

by the displacement vectors $\mathbf{d}_{jk}$, where $\mathbf{r}_{jk}$ and $\mathbf{d}_{jk}$ are vectors in three-dimensional space. For an ensemble of crystallites with identical orientations, the average diffracted intensity can be written as

$$\begin{aligned}\langle I(\mathbf{R})\rangle_d = \sum_j \sum_{j'} \sum_k \sum_{k'} \Big\langle\ & s_{\text{lat}}(\mathbf{r}_{jk}) s_{\text{lat}}(\mathbf{r}_{j'k'}) \\ & \times F_{jk}(\mathbf{R}) F^*_{j'k'}(\mathbf{R}) \\ & \times \exp[i2\pi\mathbf{R}\cdot(\mathbf{r}_{jk}+\mathbf{d}_{jk})] \\ & \times \exp[-i2\pi\mathbf{R}\cdot(\mathbf{r}_{j'k'}+\mathbf{d}_{j'k'})]\Big\rangle_d,\end{aligned} \tag{9}$$

where $\mathbf{R}$ is the position vector in reciprocal space, $F_{jk}(\mathbf{R})$ are complex amplitudes diffracted by the molecules, * denotes the complex conjugate and $s_{\text{lat}}(\mathbf{r})$ is the shape function describing the lateral cross section of the crystallite, equal to 1 inside the crystallite and 0 elsewhere.

As a result of substitution disorder, the structure factors $F_{jk}(\mathbf{R})$ differ between molecules. If lattice and substitution disorder are independent,

$$\begin{aligned}&\langle F_{jk}(\mathbf{R}) F^*_{j'k'}(\mathbf{R}) \exp[i2\pi\mathbf{R}\cdot(\mathbf{d}_{jk}-\mathbf{d}_{j'k'})]\rangle_d \\ &\quad = \langle F_{jk}(\mathbf{R}) F^*_{j'k'}(\mathbf{R})\rangle_d \langle \exp[i2\pi\mathbf{R}\cdot(\mathbf{d}_{jk}-\mathbf{d}_{j'k'})]\rangle_d.\end{aligned} \tag{10}$$

If it is assumed that the statistics for substitution disorder are stationary and that variations in the F_{jk} are uncorrelated,

$$\begin{aligned}&\langle F_{jk}(\mathbf{R}) F^*_{j'k'}(\mathbf{R})\rangle_d \\ &\quad = \begin{cases} \langle |F(\mathbf{R})|^2\rangle_d & \text{when } j=j' \text{ and } k=k', \\ |\langle F(\mathbf{R})\rangle_d|^2 & \text{otherwise.}\end{cases}\end{aligned} \tag{11}$$

If the displacement vectors $\mathbf{d}_{jk}$ (*i.e.* the lattice distortions) are uncorrelated and their statistics are stationary over the lattice, then

$$\langle \exp[i2\pi\mathbf{R}\cdot(\mathbf{d}_{jk}-\mathbf{d}_{j'k'})]\rangle_d = |\langle \exp(i2\pi\mathbf{R}\cdot\mathbf{d})\rangle_d|^2, \tag{12}$$

where $\mathbf{d}$ is a generic random vector describing the lattice distortions. Furthermore, if the displacement vectors are normally distributed with zero mean,

$$|\langle \exp(i2\pi\mathbf{R}\cdot\mathbf{d})\rangle_d|^2 = \exp(-2\pi^2\mathbf{R}\mathbf{C}\mathbf{R}^T), \tag{13}$$

where $\mathbf{C}$ is the covariance matrix of the random vector $\mathbf{d}$ and the superscript T denotes transposition (Papoulis, 1984, p. 115). Substituting (10), (11) and (13) into (9) gives

$$\begin{aligned}\langle I(\mathbf{R})\rangle_d = N\{&\langle |F(\mathbf{R})|^2\rangle_d - |\langle F(\mathbf{R})\rangle_d|^2 w_{\text{lattice}}(\mathbf{R})\} \\ &+ |\langle F(\mathbf{R})\rangle_d|^2 w_{\text{lattice}}(\mathbf{R}) \mathcal{Z}(\mathbf{R}),\end{aligned} \tag{14}$$

where N is the number of molecules in each crystallite,

$$w_{\text{lattice}}(\mathbf{R}) = \exp(-4\pi^2\mathbf{R}\mathbf{C}\mathbf{R}^T) \tag{15}$$

is the weighting due to lattice disorder and

$$\mathcal{Z}(\mathbf{R}) = \left|\sum_j \sum_k s_{\text{lat}}(\mathbf{r}_{jk}) \exp(i2\pi\mathbf{R}\cdot\mathbf{r}_{jk})\right|^2 \tag{16}$$

is the interference function of the average lattice. The first two terms in (14) describe diffuse or continuous intensity, while the third term describes a set of Bragg reflections. Since the covariance matrices of random vectors with zero mean are non-negative definite (Papoulis, 1984, p. 179), $w_{\text{lattice}}(\mathbf{R}) \leq 1$ and $w_{\text{lattice}}(\mathbf{R}) \to 0$ for $|\mathbf{R}| \to \infty$, so that the lattice disorder weight suppresses the Bragg intensities with increasing $\mathbf{R}$. It also tends to enhance the diffuse intensity with increasing $\mathbf{R}$.

The cylindrically averaged layer-line intensities, $I_l(R)$, diffracted from a fiber are obtained by substituting (14) into (7) and may be expressed as

$$I_l(R) = I_l^B(R) + I_l^D(R), \tag{17}$$

where the diffuse intensity, $I_l^D(R)$, is

$$\begin{aligned}I_l^D(R) = \langle N\rangle_s \Big\{&\langle\langle |F_l(R,\psi)|^2\rangle_d\rangle_\psi \\ &- \langle w_{\text{lattice}}(R,\psi,l/c) |\langle F_l(R,\psi)\rangle_d|^2\rangle_\psi\Big\},\end{aligned} \tag{18}$$

the Bragg intensity, $I_l^B(R)$, is

$$I_l^B(R) = \langle w_{\text{lattice}}(R,\psi,l/c)\ |\langle F_l(R,\psi)\rangle_d|^2 \langle \mathcal{Z}(\mathbf{R})\rangle_s\rangle_\psi \tag{19}$$

and the structure factors $F_l(R,\psi)$ are given by (1).

3.2. *Lattice disorder*

The elements of the covariance matrix $\mathbf{C}$ determine how the lattice disorder weight varies with ψ. To simplify evaluation of the cylindrical averages in (18) and (19), we assume that the Cartesian components (d^x, d^y, d^z) of each distortion vector vary independently of one another and that the variances of the lateral

components d^x and d^y are equal. We define the lateral and axial variances σ^2_{lat} and σ^2_{axial} as

$$\sigma^2_{\text{lat}} = \langle (d^x)^2 \rangle = \langle (d^y)^2 \rangle \quad \text{and} \quad \sigma^2_{\text{axial}} = \langle (d^z)^2 \rangle, \tag{20}$$

so that

$$\mathbf{C} = \begin{pmatrix} \sigma^2_{\text{lat}} & 0 & 0 \\ 0 & \sigma^2_{\text{lat}} & 0 \\ 0 & 0 & \sigma^2_{\text{axial}} \end{pmatrix} \tag{21}$$

and the corresponding lattice disorder weight is

$$\begin{aligned} w_{\text{lattice}}(R, \psi, Z) &= w_{\text{lattice}}(R, Z) \\ &= \exp[-4\pi^2(R^2\sigma^2_{\text{lat}} + Z^2\sigma^2_{\text{axial}})]. \end{aligned} \tag{22}$$

This is independent of ψ and can be removed from the cylindrical averages in (18) and (19). From (18) and (19), the effect of this weight is to suppress Bragg intensity with increasing R and Z, which is accompanied by an increase in diffuse intensity.

3.3. *The interference function*

Using the convolution property of Fourier transforms, one can write the interference function (16) as

$$\mathcal{Z}(\mathbf{R}) = \left| S_{\text{lat}}(\mathbf{R}) \otimes L(\mathbf{R}) \right|^2, \tag{23}$$

where $\otimes$ denotes convolution, $S_{\text{lat}}(\mathbf{R})$ is the Fourier transform of $s_{\text{lat}}(\mathbf{r})$ and $L(\mathbf{R})$ is the reciprocal-lattice function

$$L(\mathbf{R}) = (1/A_{\text{cell}}) \sum_h \sum_k \delta(\mathbf{R} - \mathbf{R}_{hk}), \tag{24}$$

where A_{cell} is the cross-sectional area of the unit cell and $\mathbf{R}_{hk}$ are the sites of the two-dimensional lattice reciprocal to (8). Substituting (24) into (23) gives

$$\begin{aligned} \mathcal{Z}(\mathbf{R}) = (1/A^2_{\text{cell}}) &\sum_h \sum_k |S_{\text{lat}}(\mathbf{R} - \mathbf{R}_{hk})|^2 \\ &+ (1/A^2_{\text{cell}}) \sum_h \sum_k \sum_{h' \neq h} \sum_{k' \neq k} S_{\text{lat}}(\mathbf{R} - \mathbf{R}_{hk}) \\ &\times S^*_{\text{lat}}(\mathbf{R} - \mathbf{R}_{h'k'}). \end{aligned} \tag{25}$$

For crystallites spanning more than a few unit cells in any direction, $S_{\text{lat}}(\mathbf{R})$ is sharply peaked at the origin and is small for all reciprocal distances of the order of one reciprocal-lattice spacing or greater. Consequently, the second term in (25) is small everywhere so that

$$\begin{aligned} \mathcal{Z}(\mathbf{R}) &\simeq (1/A^2_{\text{cell}}) \sum_h \sum_k |S_{\text{lat}}(\mathbf{R} - \mathbf{R}_{hk})|^2 \\ &= (1/A_{\text{cell}}) \left[L(\mathbf{R}) \otimes |S_{\text{lat}}(\mathbf{R})|^2 \right]. \end{aligned} \tag{26}$$

Ino & Minami (1979) have shown that (26) is exact, regardless of crystallite size, when both sides of the equation are averaged over all shifts of the shape function relative to the crystal lattice. Using (26) when calculating diffracted intensities has, therefore, the desirable effect of effectively averaging the intensity over those shifts that occur in a specimen.

For the crystallite sizes usually present in fibers, the interference function is significant only over small regions centered on the points (R_{hk}, ψ_{hk}). The structure factors $F_l(R, \psi)$ are approximately constant over these regions and equal to $F_l(R_{hk}, \psi_{hk}) = F_{hkl}$. From (19) and (26), the intensity due only to the hkl Bragg reflection is approximately

$$I^B_{hkl}(R) = (1/A_{\text{cell}}) w_{\text{lattice}}(R_{hk}, l/c) |\langle F_{hkl} \rangle_d|^2 \mathcal{P}_{hk}(R), \tag{27}$$

where $\mathcal{P}_{hk}(R)$ is the radial profile of the reflection given by

$$\mathcal{P}_{hk}(R) = (1/2\pi) \int_0^{2\pi} \langle |S_{\text{lat}}(R - R_{hk}, \psi - \psi_{hk})|^2 \rangle_s \, \mathrm{d}\psi. \tag{28}$$

The lateral shape function $s_{\text{lat}}(\mathbf{r})$ determines the reflection profiles $\mathcal{P}_{hk}(R)$ and the relative magnitudes of the Bragg and continuous intensities. In order to calculate the complete distribution of intensity along a layer line, one must, therefore, choose a form for this function. For the purpose of exploring the effects of disorder, we assume that the crystallites are all the same size and are circular in cross section. The Fourier transform of the circular shape function

$$s_{\text{lat}}(\mathbf{r}) = \begin{cases} 1 & |\mathbf{r}| \leq r_c \\ 0 & |\mathbf{r}| > r_c \end{cases} \tag{29}$$

is

$$S_{\text{lat}}(R) = r_c [J_1(2\pi r_c R)/R], \tag{30}$$

where r_c is the radius of the crystallite. When (30) is substituted into (28), $\langle \, \rangle_s$ is eliminated and the value of the integrand depends only on the distance

$$R' = R^2 + R^2_{hk} - 2RR_{hk} \cos(\psi - \psi_{hk}), \tag{31}$$

so that

$$\begin{aligned} \mathcal{P}_{hk}(R) = (r_c^2/2\pi) \int_0^{2\pi} &J_1^2(2\pi r_c [R^2 + R^2_{hk} \\ &- 2RR_{hk} \cos(\psi - \psi_{hk})]^{1/2}) \\ &\times [R^2 + R^2_{hk} - 2RR_{hk} \cos(\psi - \psi_{hk})]^{-1} \, \mathrm{d}\psi. \end{aligned} \tag{32}$$

The integral in (32) cannot be solved analytically other than for meridional reflections. A good approximation

can be obtained, however, using a method employed by Guiner (1939) and Hosemann & Bagchi (1962) in their analyses of reflection profiles. For crystallites of moderate size, this gives

$$\mathcal{P}_{00} = \pi^2 r_c^4 \exp(-\pi^2 r_c^2 R^2) \tag{33}$$

for meridional reflections and

$$\mathcal{P}_{hk}(R) \simeq (r_c^3 \pi^{1/2}/2R_{hk}) \exp[-\pi^2 r_c^2 (R - R_{hk})^2] \tag{34}$$

for non-meridional reflections.

3.4. *Thermal disorder*

At this point, it is worth considering how a description of thermal disorder may be combined with that of lattice disorder. The effects of thermal atomic motion on diffracted intensities are usually modeled by treating each atom as an independent oscillator subject to the force field exerted by the dynamically averaged crystal environment (Dunitz, Schoemaker & Trueblood, 1988). The effective potential often appears to be reasonably harmonic and at any instant the thermal displacements of equivalent atoms on different molecules are normally distributed. Because the formalism used to describe thermal disorder and lattice distortions are essentially the same, it has often been assumed that the effects of the two forms of disorder are indistinguishable (see, for example, Fraser & MacRae, 1973, p. 73). The important difference between the two components of disorder is that lattice distortions involve displacement of each molecule as a rigid body, whereas thermal disorder involves, at least approximately, independent displacements of the individual atoms. Lattice distortions, as modeled here, do not disrupt the axial periodicity of each molecule so that the diffracted intensity is restricted to layer lines. Uncorrelated thermal motions of the individual atoms, however, destroy the periodicity of the molecule from one instant to the next so that intensity is removed from the layer lines and dispersed continuously throughout reciprocal space.

Assuming that all of the atoms in a polymer have identical thermal displacement parameters (an assumption that is usually made in fiber diffraction analysis since the number of data is not adequate to assign thermal parameters to individual atoms) and performing a similar analysis to that for lattice distortions shows that the intensity diffracted when there is thermal disorder is given by

$$\langle I(R,Z)\rangle = I_t(R,Z) + w_t(R,Z)\langle I(R,Z)\rangle_d, \tag{35}$$

where

$$w_t(R,Z) = \exp[-4\pi^2\sigma_t^2(R^2+Z^2)] \tag{36}$$

is the thermal disorder weight and σ_t is the mean squared displacement of each atom due to thermal motion,

$$I_t(R,Z) = N[1 - w_t(R,Z)] \sum_p f_p^2 (R^2+Z^2)^{1/2} \tag{37}$$

is the diffuse intensity due to thermal disorder and $\langle I(R,Z)\rangle_d$ is the intensity diffracted in the absence of thermal disorder. Reference to (36) and (37) shows that the diffuse intensity due to thermal disorder is distributed isotropically throughout reciprocal space. This intensity is subtracted out as a component of the background intensity, and hence the effect of thermal disorder can be modeled by simply multiplying the layer-line intensities by the isotropic factor $w_t(R,Z)$.

3.5. *Probability density functions for helical molecules*

Substitution disorder involving rotations φ and axial translations z is specified by a probability density $p(\varphi, z)$ defined over all distinguishable states of the helical molecules. A helical molecule is periodic in (φ, z) space and is invariant under the transformations

$$\begin{aligned} \varphi' &= \varphi + 2\pi k_1 v/u + 2\pi k_2 \\ z' &= z + k_1 c/u, \end{aligned} \tag{38}$$

where k_1 and k_2 are any integers. Using this transformation pair, any (φ, z) can be mapped into the region

$$0 \le \varphi < 2\pi, \quad 0 \le z < c/u \tag{39}$$

and this, therefore, is the region on which $p(\varphi, z)$ should be specified. If, however, distributions for (φ, z) are defined on infinite intervals, the implications of the periodic nature of the molecule must be considered.

It is often convenient to define a density function $p'(\varphi', z')$ for φ' and z' taking all real values (a normal distribution for example). Many of the states (φ', z') then correspond to a single state (φ, z) satisfying (39). The actual density function $p(\varphi, z)$ of distinguishable states is given by

$$p(\varphi,z) = \sum_{k_1}\sum_{k_2} p'(\varphi + 2\pi k_1 v/u + 2\pi k_2, z + k_1 c/u). \tag{40}$$

This distribution consists of many copies of the specified function $p'(\varphi, z)$ folded, or aliased, back into the region of (φ, z) space given by (39). For a molecule with high helix symmetry (u large and v small), the effect of this aliasing will be more pronounced than for a molecule with low symmetry. For normal distributions, we specify $p'(\varphi', z')$ and, provided the variances of φ' and z' are small, the actual distribution $p(\varphi, z) \simeq p'(\varphi, z)$. If the variances are large, however, the actual distribution given by (40) can be quite different to $p'(\varphi', z')$. Specific implications of this are described later.

3.6. *Substitution disorder*

The effects of substitution disorder are expressed in (18) and (19) through terms involving the averages $\langle\langle|F_l(R,\psi)|^2\rangle_d\rangle_\psi$, $|\langle F_l(R,\psi)\rangle_d|^2$ and $\langle|\langle F_l(R,\psi)\rangle_d|^2\rangle_\psi$. These effects are expressed here using substitution disorder weights calculated from the probability densities of the rotations and axial displacements of the molecules. Axial translations with normal distributions are already included in the model as a component of lattice disorder. However, translations that are completely random or are coupled to rotations are best regarded as components of substitution disorder.

Using (1) and (2), the complex amplitude diffracted by a molecule rotated about its axis through an angle φ and translated a distance z along this axis can be written in terms of the $G_{nl}(R)$ of a reference molecule as

$$F_l(R,\psi) = \exp(i2\pi zl/c) \times \sum_n G_{nl}(R)\exp[in(\psi-\varphi+\pi/2)]. \tag{41}$$

The cylindrical average $\langle\langle|F_l(R,\psi)|^2\rangle_d\rangle_\psi$ appearing in (18) is then

$$\langle\langle|F_l(R,\psi)|^2\rangle_d\rangle_\psi = \sum_n\sum_m\{G_{nl}(R)G^*_{ml}(R)\exp[i(n-m)\pi/2] \times \langle\exp[-i(n-m)\varphi]\rangle_d\langle\exp[i(n-m)\psi]\rangle_\psi\}. \tag{42}$$

The average over ψ on the right-hand side of (42) vanishes unless $m = n$, so that

$$\langle\langle|F_l(R,\psi)|^2\rangle_d\rangle_\psi = \sum_n |G_{nl}(R)|^2, \tag{43}$$

regardless of how φ and z are distributed.

The average complex amplitude diffracted by a molecule can be written as

$$\langle F_l(R,\psi)\rangle_d = \sum_n w_{nl}G_{nl}(R)\exp[in(\psi+\pi/2)], \tag{44}$$

where w_{nl}, the *substitution disorder weight*, is defined as

$$w_{nl} = \int_0^{c/u}\int_0^{2\pi} p(\varphi,z)\exp[i(2\pi zl/c - n\varphi)]\,d\varphi\,dz. \tag{45}$$

For independent rotations and translations of the molecules, the probability density function $p(\varphi,z)$ factorizes as

$$p(\varphi,z) = p_\varphi(\varphi)p_z(z), \tag{46}$$

so that the disorder weight can be factorized as

$$w_{nl} = w^\varphi_n w^z_l, \tag{47}$$

where

$$w^\varphi_n = \int_0^{2\pi} p_\varphi(\varphi)\exp(-in\varphi)\,d\varphi \tag{48}$$

and

$$w^z_l = \int_0^{c/u} p_z(z)\exp(i2\pi zl/c)\,dz. \tag{49}$$

Equation (45) gives the substitution disorder weight in terms of the density function $p(\varphi,z)$ of distinguishable states. If, instead of $p(\varphi,z)$, a density function $p'(\varphi',z')$ defined on the infinite interval is used to describe substitution disorder, the corresponding disorder weights are obtained by substituting (40) into (45) as

$$w_{nl} = \int_0^{c/u}\int_0^{2\pi}\sum_{k_1}\sum_{k_2} p'(\varphi+2\pi k_1 v/u+2\pi k_2, z+k_1c/u) \times \exp[i(2\pi zl/c - n\varphi)]\,d\varphi\,dz. \tag{50}$$

Using (38) to make a change of variables, one can write (50) as

$$w_{nl} = \sum_{k_1}\sum_{k_2}\left\{\int_{k_1c/u}^{(k_1+1)c/u}\int_{2\pi k_1v/u+2\pi k_2}^{2\pi k_1v/u+2\pi(k_2+1)} p'(\varphi',z') \times \exp[i(2\pi z'l/c - n\varphi')] \times \exp[i2\pi k_1(nv-l)/u]\,d\varphi'\,dz'\right\}. \tag{51}$$

From the helix selection rule (3), $[nv-l]/u$ is equal to an integer, so that the second exponential in (51) is equal to unity. Evaluating the sums gives

$$w_{nl} = \int_{-\infty}^{\infty}\int_{-\infty}^{\infty} p'(\varphi',z')\exp[i(2\pi z'l/c - n\varphi')]\,d\varphi'\,dz', \tag{52}$$

which has the same form as (45). The correct disorder weights are therefore calculated using (52) when the density $p'(\varphi',z')$ is used.

It follows from (44) that

$$\langle|\langle F_l(R,\psi)\rangle_d|^2\rangle_\psi = (1/2\pi)\sum_n\sum_m\left\{w_{nl}w^*_{ml}G_{nl}(R) \times G^*_{ml}(R)\exp[i(n-m)\pi/2] \times \int_0^{2\pi}\exp[i(n-m)\psi]\,d\psi\right\} \tag{53}$$

and the integral over ψ vanishes unless $n = m$, so that

$$\langle|\langle F_l(R,\psi)\rangle_d|^2\rangle_\psi = \sum_n |w_{nl}|^2|G_{nl}(R)|^2. \tag{54}$$

Substituting (43) and (54) into (18) gives the diffuse intensity as

$$I^D_l(R) = \langle N\rangle_s\sum_n |G_{nl}(R)|^2[1-|w_{nl}|^2 w_{\text{lattice}}(R,l/c)], \tag{55}$$

while substituting (44) into (27) gives

$$I^B_{hkl}(R) = (1/A^2_{\text{cell}}) w_{\text{lattice}}(R_{hk}, l/c) \times \left| \sum_n w_{nl} G_{nl}(R_{hk}) \times \exp[in(\psi_{hk} + \pi/2)] \right|^2 \mathcal{P}_{hk}(R) \quad (56)$$

for the corresponding Bragg intensity. Equations (55) and (56) are the general expressions we seek for diffraction from a polycrystalline fiber incorporating lattice and substitution disorder. To further evaluate the implications of these equations, the weights w_{nl} are calculated for specific kinds of disorder.

3.6.1. *Combined disorder.* It is sometimes convenient to consider disorder as having two or more components, each involving rotations and translations that are independent of the rotations and translations of the other components. Suppose that two such disorder components are described by the density functions $p_1(\varphi_1, z_1)$ and $p_2(\varphi_2, z_2)$ with respective weights $w^{(1)}_{nl}$ and $w^{(2)}_{nl}$. When the two disorders are combined, a molecule has rotations $\varphi = \varphi_1 + \varphi_2$ and translations $z = z_1 + z_2$, where φ_1 is independent of φ_2 and z_1 is independent of z_2. If the density functions are defined on the infinite interval, standard probability theory (Papoulis, 1984, p. 135) gives the density function $p(\varphi, z)$ of the combined disorder as

$$p(\varphi, z) = \int_{-\infty}^{\infty} \int_{-\infty}^{\infty} p_1(\varphi - \varphi', z - z') p_2(\varphi', z') \, \mathrm{d}\varphi' \, \mathrm{d}z', \quad (57)$$

i.e. the convolution of the individual density functions. Since w_{nl} and $p(\varphi, z)$ are a Fourier transform pair, it follows from the convolution theorem that the corresponding disorder weight for $p(\varphi, z)$ is

$$w_{nl} = w^{(1)}_{nl} w^{(2)}_{nl}. \quad (58)$$

If, however, p_1 and p_2 are the actual densities of distinguishable states, substitution of (40) into (57) shows that the probability density function for the combined disorder is given by

$$p(\varphi, z) = \int_0^{c/u} \int_0^{2\pi} p_1(\varphi - \varphi', z - z') p_2(\varphi', z') \, \mathrm{d}\varphi' \, \mathrm{d}z', \quad (59)$$

where $p_1(\varphi, z)$ is extended by periodic repetition to arguments outside the interval on which it is defined, *i.e.* (59) is a circular convolution. When (59) is substituted into (45), the weight for the combined disorder is again given by (58).

3.6.2. *Small rotations.* The effect of small rotations that are independent of axial translations is examined by assigning a normal distribution, with standard deviation σ_φ, to φ. This distribution is aliased by molecular symmetry into the interval $(0, 2\pi)$ in accordance with (40). Provided that $\sigma_\varphi << 2\pi$, the effect of aliasing is small and the actual distribution of distinguishable states is approximately normal. Substituting the normal distribution into (48) gives

$$w^\varphi_n = \exp(-n^2 \sigma^2_\varphi / 2) \quad (60)$$

as the weighting due to small rotations. Equations (55), (56) and (60) show that the effect of small rotations is to suppress the contribution of the higher-order Fourier–Bessel coefficients to the Bragg intensity and correspondingly to increase the diffuse intensity.

3.6.3. *Random rotations.* If the molecules are randomly rotated, then $p_\varphi(\varphi) = (2\pi)^{-1}$ and

$$w^\varphi_n = (1/2\pi) \int_0^{2\pi} \exp(in\varphi) \, \mathrm{d}\varphi = \delta_{n0}, \quad (61)$$

where δ_{ij} is the Kronecker delta. Since $n = 0$ is a solution to the helix selection rule only on layer lines $l = mu$, where m is an integer, substituting (61) into (55) and (56) gives

$$I^D_l(R) = \langle N \rangle_s \sum_n \{ |G_{nl}(R)|^2 - \delta_{n0} |G_{0l}(R)|^2 \times \exp[-4\pi^2 (R^2 \sigma^2_{\text{lat}} + Z^2 \sigma^2_{\text{axial}})] \} \quad (62)$$

and

$$I^B_{hkl}(R) = \begin{cases} [\mathcal{P}_{hk}(R)/A^2_{\text{cell}}] |G_{0l}(R_{hk})|^2 \times \exp[-4\pi^2 (R^2 \sigma^2_{\text{lat}} + Z^2 \sigma^2_{\text{axial}})] & l = um \\ 0 & l \neq mu, \end{cases} \quad (63)$$

respectively. Therefore, random rotations eliminate Bragg reflections from all layer lines other than those for which $l = mu$. Diffuse intensity is excluded from layer lines for which $l = mu$ provided there is no lattice disorder; otherwise, diffuse intensity appears on these layer lines, particularly at large values of R.

3.6.4. *Random axial translations.* For random axial translations, $p_z(z) = 1/c$ on the interval $0 \leq z < c$ and substituting into (49) gives $w^z_l = \delta_{l0}$. Substituting this weight into (55) and (56) gives

$$I^D_l(R) = \begin{cases} \langle N \rangle_s \sum_n |G_{n0}(R)|^2 \times [1 - \exp(-4\pi^2 R^2 \sigma^2_{\text{lat}})] & l = 0 \\ \langle N \rangle_s \sum_n |G_{nl}(R)|^2 & l \neq 0 \end{cases} \quad (64)$$

and

$$I^B_{hkl}(R) = \begin{cases} [\mathcal{P}_{hk}(R)/A^2_{\text{cell}}] \exp(-4\pi^2 R^2 \sigma^2_{\text{lat}}) \\ \quad \times \sum_n |G_{n0}(R) \exp[in(\psi_{hk} + \pi/2)]|^2 & l = 0 \\ 0 & l \neq 0, \end{cases} \tag{65}$$

respectively. These equations are similar to those for random rotations. They show, however, that Bragg reflections occur only on the equator, rather than on all the layer lines $l = mu$ as in the case of random rotations. In addition, all Bessel orders satisfying the helix selection rule contribute to the Bragg reflections on the equator, rather than just the zero order.

3.6.5. *Random rotations and axial translations.* Randomly rotated polymers are unlikely to be in register so that random rotations are likely to be accompanied by random axial translations. The diffracted intensities are then

$$I^D_l(R) = \begin{cases} \langle N \rangle_s \left[\sum_n |G_{n0}(R)|^2 - |G_{00}(R)|^2 \right. \\ \quad \left. \times \exp(-4\pi^2 R^2 \sigma^2_{\text{lat}}) \right] & l = 0 \\ \langle N \rangle_s \sum_n |G_{nl}(R)|^2 & l \neq 0 \end{cases} \tag{66}$$

and

$$I^B_{hkl}(R) = \begin{cases} [\mathcal{P}_{hk}(R)/A^2_{\text{cell}}] \\ \quad \times \exp(-4\pi^2 R^2 \sigma^2_{\text{lat}}) |G_{00}(R)|^2 & l = 0 \\ 0 & l \neq 0, \end{cases} \tag{67}$$

respectively, so that Bragg reflections occur only on the equator and their intensities are determined only by the zero-order Fourier–Bessel structure factor.

3.6.6. *Discrete rotations and translations.* If the molecules at each lattice site can have one of M different positions (φ_i, z_i) relative to a reference molecule, with probabilities p_i, then

$$p(\varphi, z) = \sum_{i=1}^{M} p_i \delta(\varphi - \varphi_i, z - z_i) \tag{68}$$

and the disorder weight is

$$w_{nl} = \sum_{i=1}^{M} p_i \exp(i2\pi z_i l/c - in\varphi_i). \tag{69}$$

The effect of this weight partly depends on the phase of the $G_{nl}(R)$ to which it is applied. A relatively simple case to consider is that where a molecule is equally likely to adopt one of two positions, $(\varphi_1, z_1) = (0, 0)$ and $(\varphi_2, z_2) = (\varphi', z')$. The disorder weight is then

$$w_{nl} = \tfrac{1}{2}\{1 + \exp[i(2\pi z' l/c - n\varphi')]\}. \tag{70}$$

Reference to (56) shows that the effect of this weight is to remove the contribution of the nth-order Bessel function to the Bragg intensity wherever $(2\pi z' l/c - n\varphi') \simeq k\pi$ for k an odd integer. At positions where this condition is satisfied and only one Bessel order is significant (in the vicinity of the meridian, for example), Bragg intensity is eliminated entirely. The contribution of $G_{nl}(R)$ to the diffuse intensity tends to be suppressed where $(2\pi z' l/c - n\varphi') \simeq k\pi$, where k is an even integer, although this also depends on what lattice disorder is present.

3.6.7. *Screw disorder.* Screw disorder consists of rotations of the molecules that are coupled to axial translations. This form of disorder was first proposed by Franklin & Klug (1956) as an explanation for the differences between diffraction patterns obtained from wet and dry fibers of tobacco mosaic virus. It has been suggested (Klug & Franklin, 1958; Marvin, Spencer, Wilkins & Hamilton, 1961; Arnott, 1980) that DNA fibers with diffraction patterns containing Bragg reflections only near the center of the pattern may be 'screw disordered'.

Screw rotations are most conveniently described by factorizing the joint probability density $p(\varphi, z)$ as

$$p(\varphi, z) = p(z|\varphi) p(\varphi), \tag{71}$$

where $p(z|\varphi)$ denotes the distribution of z conditional on φ and specifies the coupling between the translations and rotations of the molecules. A pure screw disorder is specified by

$$p(z|\varphi) = \delta[z - \varphi(P_s/2\pi)], \tag{72}$$

where P_s is the pitch of the screw rotations. In practice, P_s is probably determined by the pattern of helical grooves and protuberances on the surface of each molecule and the pattern of interlocking between adjacent molecules that they give rise to. One expects that the helix symmetry of these surface features would usually be the same as that of the molecule but this need not always be the case (Klug & Franklin, 1958).

For small screw rotations, φ is assigned a normal distribution with standard deviation σ_φ. Equations (71), (72) and (45) show that

$$w_{nl} = \exp[-\sigma^2_\varphi (n - lP_s/c)^2/2]. \tag{73}$$

At any radius R, the weights of the Bragg and diffuse components depend on the relationship between n and l. Referring to (56) and (55) shows that the Bragg intensity receives the greatest contribution from the orders for which $|n - lP_s/c|$ is smallest and the contributions from all other orders decreases as $|n - lP_s/c|$ increases. The

contributions of the different Bessel orders to the diffuse component increases with increasing $|n - lP_s/c|$. If the pitch P_s of the screw disorder is equal to the pitch $P = c/v$ of the molecular helix, the maximum contribution to the Bragg intensity comes from the Bessel orders $n = l/v$ and correspondingly this order makes no contribution to the diffuse intensity. Note that solutions to the selection rule for $l < 0$ are just those for $l > 0$ with the signs reversed so that the effect of screw disorder on layer lines with $l < 0$ is identical to that on the layer lines with $l > 0$.

For random screw disorder, $p(\varphi) = 1/2\pi$ for $0 \leq \varphi < 2\pi$, so that

$$w_{nl} = (1/2\pi) \int_0^{2\pi} \exp[-i(n - lP_s/c)\varphi]\, d\varphi = \delta_{n,lP_s/c}. \tag{74}$$

Substitution of (74) into (55) and (56) gives the diffuse and Bragg intensities as

$$I_l^D(R) = \langle N \rangle_s \sum_n |G_{nl}(R)|^2 \times [1 - \delta_{n,lP_s/c} \exp(-4\pi^2 R^2 \sigma_{\text{lat}}^2)] \tag{75}$$

and

$$I_{hkl}^B(R) = [\mathcal{P}_{hk}(R)/A_{\text{cell}}] \exp(-4\pi^2 R^2 \sigma_{\text{lat}}^2) \times \left| \sum_n \delta_{n,lP_s/c} G_{nl}(R_{hk}) \times \exp[in(\psi_{hk} + \pi/2)] \right|^2, \tag{76}$$

respectively. In this case, only the Bessel order $n = lP_s/c$ contributes to the Bragg intensity and then only when n satisfies the helix selection rule. Other orders satisfying the selection rule contribute only to the diffuse intensity. If $P_s = P$, then only the order $n = l/v$ contributes to the Bragg reflections on layer line l. Previous statements that only the $n = l$ Bessel order contributes to the Bragg reflections in the presence of screw disorder (Arnott, 1980) are true only if $P_s = P$ and the helix is integral ($v = 1$).

3.6.8. *Directional disorder.* Most biopolymers have an absolute direction or sense, and in a disordered crystallite may pack with random direction. If the complex amplitude diffracted by a reference 'up' molecule is

$$F_l^{\text{up}}(R, \psi) = \sum_n G_{nl}(R) \exp[in(\psi + \pi/2)], \tag{77}$$

then that diffracted by a 'down' molecule is

$$F_l^{\text{down}}(R, \psi) = \sum_n G_{nl}^*(R) \exp[i(4\pi z_0 l/c - 2n\varphi_0)] \times \exp[in(\psi + \pi/2)], \tag{78}$$

where a down molecule is generated from an up molecule by a 180° rotation about the axis defined by $\varphi = \varphi_0$ and $z = z_0$.

If one assumes that it is equally probable for a molecule to be pointing either up or down, the average intensity diffracted from a molecule is given by

$$\langle |F_l(R, \psi)|^2 \rangle_d = \tfrac{1}{2} [|F_l^{\text{up}}(R, \psi)|^2 + |F_l^{\text{down}}(R, \psi)|^2]. \tag{79}$$

When cylindrically averaged, (79) reduces to (43). This is also true if one of the other types of disorder discussed above is present. If it is assumed that this is the case, the average complex amplitude diffracted by a molecule is

$$\langle F_l(R, \psi) \rangle_d = \tfrac{1}{2} \sum_n (w_{nl} \{G_{nl}(R) + G_{nl}^*(R) \times \exp[i(4\pi z_0 l/c - 2n\varphi_0)]\} \times \exp[in(\psi + \pi/2)]) \tag{80}$$

and it follows that

$$\langle |\langle F_l(R, \psi) \rangle_d|^2 \rangle_\psi = \sum_n |w_{nl}|^2 |\Re\{G_{nl}(R) \exp(\beta_{nl})\}|^2, \tag{81}$$

where $\Re$ denotes the real part and

$$\beta_{nl} = n\varphi_0 - 2\pi z_0 l/c. \tag{82}$$

The diffuse intensity is obtained by substituting (43) and (81) into (55) as

$$I_l^D(R) = \langle N \rangle_s \sum_n |G_{nl}(R)|^2 - \langle N \rangle_s w_{\text{lattice}}(R, l/c) \times \sum_n |w_{nl}|^2 [\Re\{G_{nl}(R) \exp(i\beta_{nl})\}]^2. \tag{83}$$

Using (79) to calculate $\langle |F_{hkl}|^2 \rangle_d$ and substituting the result into (27) gives the associated Bragg intensity as

$$I_{hkl}^B(R) = [\mathcal{P}_{hk}(R)/A_{\text{cell}}^2] w_{\text{lattice}}(R, l/c) \times \left| \sum_n w_{nl} \Re\{G_{nl}(R_{hk}) \times \exp[in(\psi_{hk} + \pi/2)] \exp(i\beta_{nl})\} \right|^2. \tag{84}$$

The effects of directional disorder are not confined to any particular region of reciprocal space and depend on the values of φ_0 and z_0 and on the phase of the individual Fourier–Bessel structure factors. Only the contribution of $G_{00}(R)$ to the Bragg intensity is unaffected.

3.7. *Disorientation and finite coherence length*

The layer-line intensities derived above are the intensities diffracted from an ideal specimen in which the constituent crystallites are perfectly oriented and are composed of structurally regular molecules of infinite length. In real specimens, the coherence length

of the molecules (or structurally regular segments of molecules) that aggregate to form crystallites is finite, and they diffract bands of intensity rather than sharp layer lines. Crystallite disorientation smears these bands along arcs centered on the origin of reciprocal space (Holmes & Barrington Leigh, 1974).

The distribution in the inclination of the crystallites can be described by an orientation density function $N(\alpha)$ such that $N(\alpha)\,\mathrm{d}\omega$ is the fraction of the crystallites with their long axes contained in an element of solid angle $\mathrm{d}\omega$ at an inclination α to the fiber axis. The exact form of $N(\alpha)$ depends on the factors giving rise to disorientation and is usually not known (Fraser, MacRae, Miller & Rowlands, 1976). In many cases, however, angular reflection profiles calculated for a Gaussian orientation density function appear to match measured profiles reasonably accurately (Fraser, MacRae, Miller & Rowlands, 1976). Provided the variance, α_0, of the angle of orientation is small, the intensity diffracted from a fiber is then given by (Holmes & Barrington Leigh, 1974)

$$I(\rho,\sigma) = \sum_l \int_0^\pi I_p(\rho,\sigma') \exp[-(\sigma-\sigma')^2/2\alpha_0^2] \times i_0(\sin\sigma \sin\sigma'/\alpha_0^2) \sin\sigma'\,\mathrm{d}\sigma', \quad (85)$$

where (ρ,ψ,σ) are spherical polar coordinates in reciprocal space; $I_p(\rho,z)$ is the cylindrically averaged intensity diffracted in the absence of disorientation which is given by

$$I_p(\rho,\sigma) = \sum_l I_l(R)\mathcal{P}_{\text{axial}}(Z-l/c)\Big|_{R=\rho\sin\sigma,\ Z=\rho\cos\sigma}, \quad (86)$$

where $\mathcal{P}_{\text{axial}}(Z)$ is the axial layer-line profile; and $i_0(x)$ is given by

$$i_0(x) = \exp(-x) I_0(x), \quad (87)$$

where $I_0(x)$ is the modified Bessel function of the second kind of order zero (Abramowitz & Stegun, 1972, p. 374). The layer-line profile $\mathcal{P}_{\text{axial}}(Z)$ is generally approximated as

$$\mathcal{P}_{\text{axial}}(Z) = \exp(-\pi^2 l_c^2 Z^2), \quad (88)$$

where l_c is the coherence length (Stubbs, 1974). Layer-line intensities calculated using the expressions developed in the preceding sections may be substituted into (86) and a two-dimensional diffraction pattern calculated numerically using (85).

4. Simulations

To examine the implications of the theory described above and to show specific examples of the relationships between disorder and the resulting diffraction effects, layer-line amplitudes were calculated for models of a polycrystalline fiber incorporating various kinds of disorder using the equations derived in this paper. Results of simulations of diffracted intensities may be presented either as plots of the intensity $I_l(R)$ on each layer line, or as continuous tone representations of the intensity $I(\rho,\sigma)$ on an entire diffraction pattern. We have found that the detailed features in the diffraction pattern tend to be less discernible in the latter representation, and so we use plots of layer-line amplitudes $I_l^{1/2}(R)$ to present most of the results in this section. Several representative two-dimensional simulated patterns are, however, shown at the end of this section.

The molecule used for the calculations was the polynucleotide duplex poly(dA)·poly(rU), which has 11_1 helix symmetry and packs, on average, in a trigonal unit cell with $a = b = 24.8$ and $c = 33.7$ Å (Arnott, Chandrasekaran, Millane & Park, 1986). Fourier–Bessel structure factors were calculated from the atomic coordinates using 'water-weighted' atomic scattering factors (Fraser, MacRae & Suzuki, 1978) and layer-line amplitudes calculated out to 3.0 Å resolution ($\rho_{\max} = 0.33$ Å^{-1}). The radius of the crystallites, r_c, was set to 200 Å, and the temperature factor $B = 4\pi^2\sigma_t^2$ to 6 Å^2.

Fig. 2 shows the diffracted amplitude calculated for an ideal polycrystalline fiber. Including lateral and axial disorder with $\sigma_{\text{lat}} = \sigma_{\text{axial}} = 1$ Å (Fig. 3*a*) downweights the Bragg component of the diffracted amplitude with increasing R and Z. The Bragg reflections are substantially reduced on the higher layer lines and at the periphery of the diffraction pattern and there is a concomitant increase in the amplitude of the diffuse component.

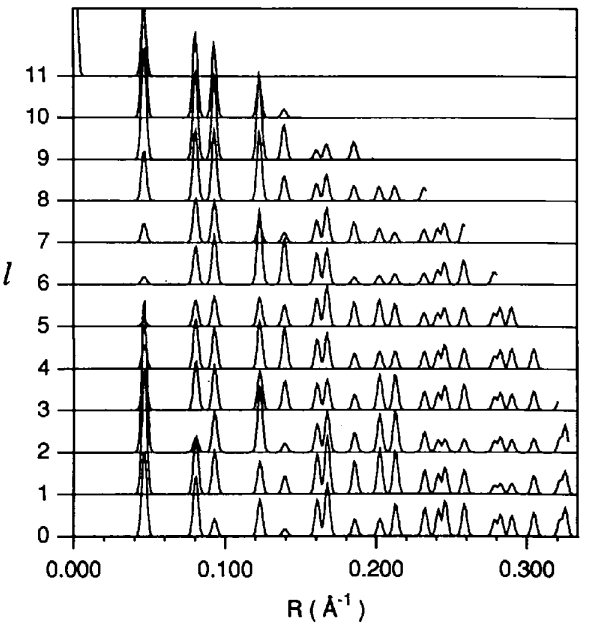

Fig. 2. Calculated layer-line amplitudes for an ideal polycrystalline fiber.

Diffuse amplitude also appears close to the center of the pattern because although the weight it receives in this region is small the amplitude of the molecular transform $F_l(R, \psi)$ is large. Increasing both σ_{lat} and σ_{axial} to 2 Å contracts the region of reciprocal space in which Bragg reflections occur as shown in Fig. 3(*b*).

Diffraction from a specimen in which the molecules are subject only to normally distributed rotations with $\sigma_\varphi = 10°$ is shown in Fig. 4(*a*). Rotational disorder reduces the contribution of the higher-order Fourier–Bessel structure factors to the Bragg intensity on each layer line and increases their contribution to the diffuse intensity. The Bragg reflections are most intense on layer lines with an index close to 0 and 11, since on these layer lines the helix selection rule has solutions that are close to zero. The maximum radius

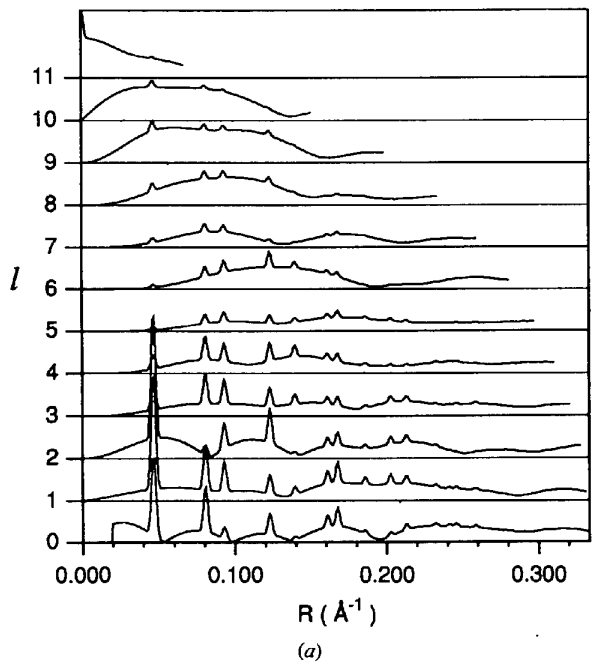

(*a*)

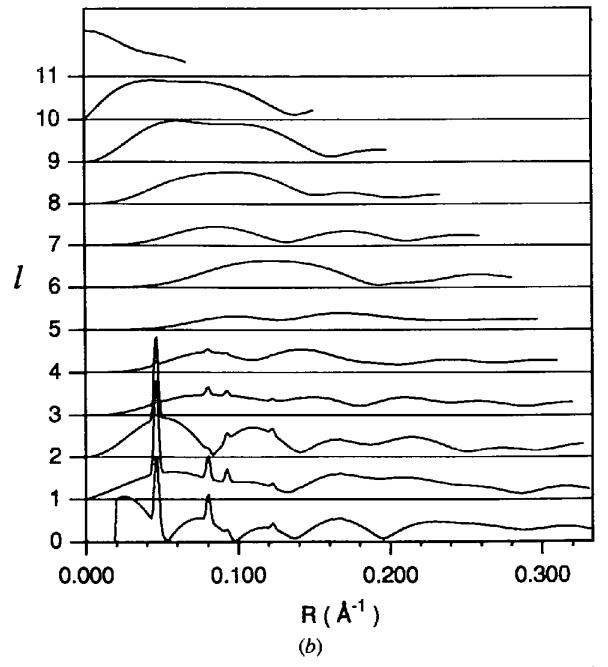

(*b*)

Fig. 3. Calculated layer-line amplitudes for small lateral and axial displacements of the molecules with (*a*) $\sigma_{\text{lat}} = \sigma_{\text{axial}} = 1$ Å and (*b*) $\sigma_{\text{lat}} = \sigma_{\text{axial}} = 2$ Å.

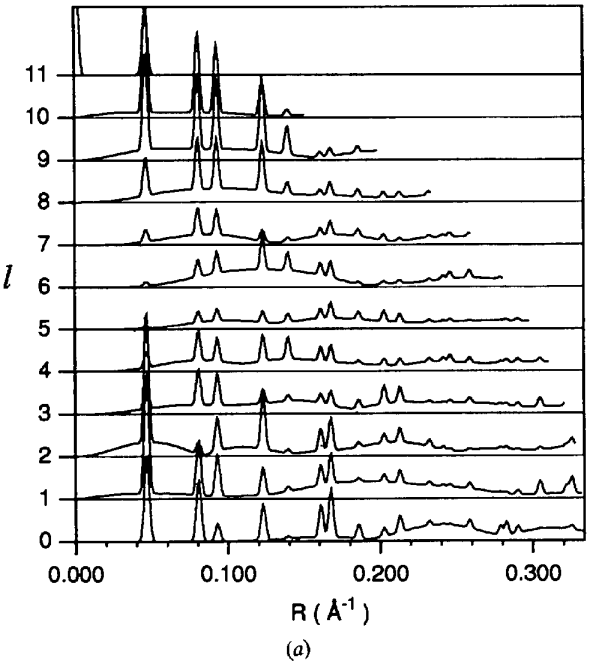

(*a*)

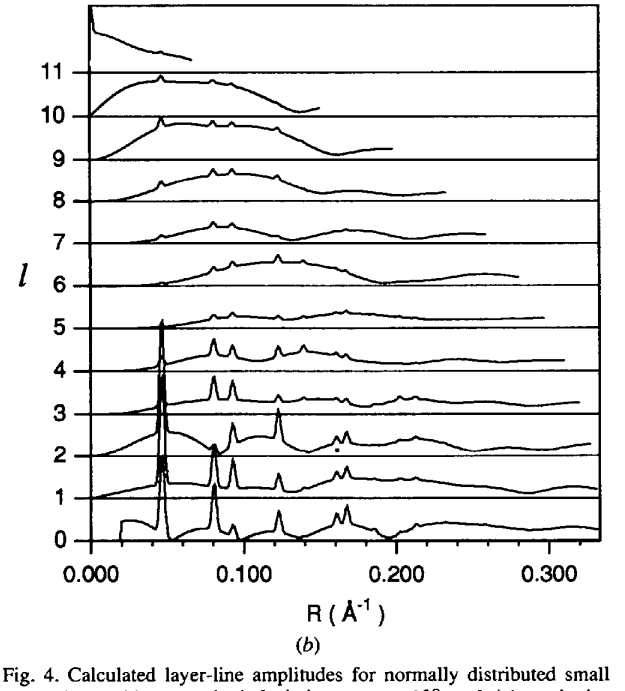

(*b*)

Fig. 4. Calculated layer-line amplitudes for normally distributed small rotations with a standard deviation $\sigma_\varphi = 10°$ and (*a*) no lattice disorder, and (*b*) lattice disorder with $\sigma_{\text{lat}} = \sigma_{\text{axial}} = 1$ Å.

of the molecule is about 12 Å, so that, from (4), only $G_{00}(R)$ is significant on the equator for $R \lesssim 0.14\,\text{Å}^{-1}$. From (60), the weight w_n^{φ} is zero for $n = 0$, so that the intensity of the four Bragg reflections on the equator are unaffected by rotation disorder, and continuous intensity is absent for $R \lesssim 0.14\,\text{Å}^{-1}$. This also occurs on layer line $l = 11$.

The effect of adding small axial and lateral translations with $\sigma_{\text{axial}} = \sigma_{\text{lat}} = 1$Å to the small rotations is shown in Fig. 4(*b*). The amplitudes of the Bragg reflections are further reduced with distance from the meridian and the equator. Near the center of the pattern, where rotation disorder has little or no effect, the effects of the lattice distortions dominate and there is increased

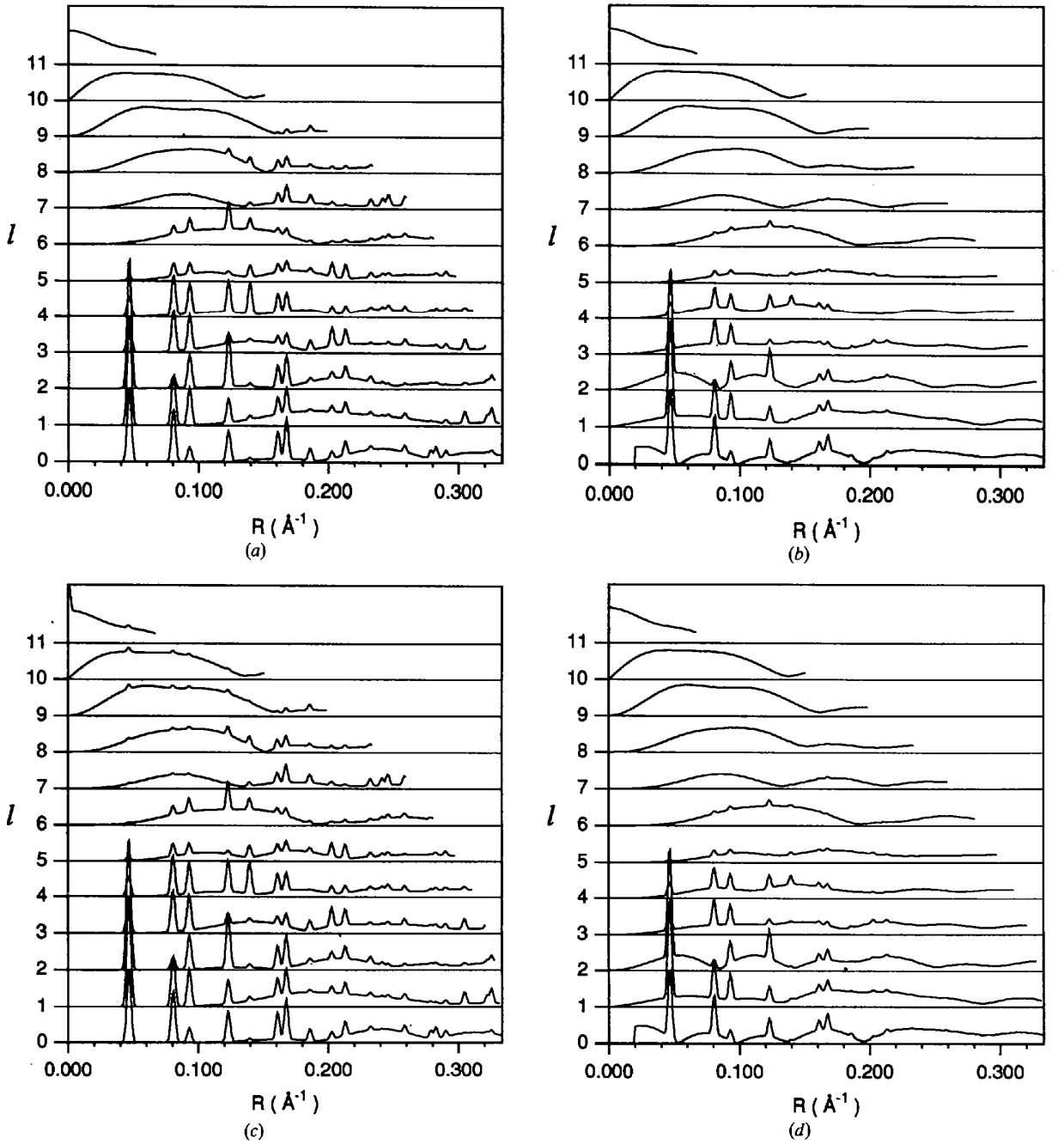

Fig. 5. Calculated layer-line amplitudes for a polycrystalline fiber with (*a*) random screw disorder and no lattice disorder, (*b*) random screw disorder and lattice disorder with $\sigma_{\text{lat}} = \sigma_{\text{axial}} = 1$ Å, (*c*) small screw disorder with $\sigma_{\varphi} = 10°$ and no lattice disorder, and (*d*) small screw disorder with $\sigma_{\varphi} = 10°$ and lattice disorder with $\sigma_{\text{lat}} = \sigma_{\text{axial}} = 1$ Å.

diffuse intensity relative to that produced by rotation disorder alone.

For a molecule with high helix symmetry, the effects of rotations are more pronounced at large values of R, where high-order $G_{nl}(R)$ terms contribute to the diffracted intensity, than at small values of R, where only low-order terms contribute. However, the Bragg reflections that occur at these radii are those most affected by lateral disorder. When there is both lattice disorder and rotational disorder, the effects of rotation are mainly evident on those layer lines for which the main contribution to the diffracted amplitude comes from $G_{nl}(R)$ terms of moderate order, provided that the Bragg reflections have not already been removed by axial disorder. For example, comparing the pattern for small rotations and lattice disorder (Fig. 4*b*) with that for lattice distortions only (Fig. 3*a*) shows that the effects of small rotations are most apparent on layer lines $l = 3$, 4 and 5 where the Bragg reflections are downweighted more than they are for lattice distortions only. The rotations also remove the weak reflections at large R that appear on layer lines $l = 0$, 1 and 2 of the pattern for lattice distortions only.

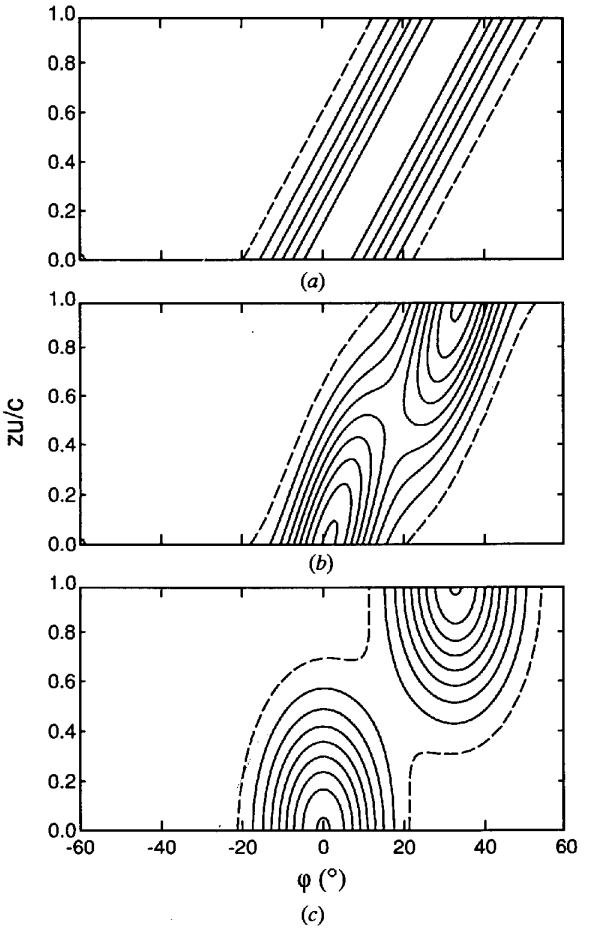

Fig. 6. Probability density functions $p(\varphi, z)$ for the molecular positions, for axial translations with $\sigma_{\text{axial}} = 1$ Å, and (*a*) random screw disorder, (*b*) small screw rotations with $\sigma_\varphi = 10°$, and (*c*) small rotations with $\sigma_\varphi = 10°$. The first contour level (broken line) is at 0.1 and the increment between levels is 0.1.

The effect of screw disorder depends on the relationship between the pitch of the screw and the pitch of the molecular helix. We assume here that these two pitches are equal. The effects of random screw disorder are shown in Fig. 5(*a*). On each layer line, only the Fourier–Bessel structure factors of order $n = l$ contribute to the Bragg intensity. On layer lines $l \leq 5$, this Bessel order is dominant at small values of R, so that the Bragg reflections in the low-resolution region of the diffraction pattern are not affected. On layer lines $l \geq 6$, the Bessel order n that is significant for R small is not equal to l and only diffuse intensity appears in this region. Bragg reflections appear further from the meridian where the structure factor of order $n = l$ becomes significant.

Fiber diffraction patterns with Bragg reflections restricted to the low-resolution region have often been attributed to screw disorder, on the basis of the oversimplified argument that only the Fourier–Bessel structure factors of order $n = l$ contribute at low resolution and produce Bragg reflections only in this region (Arnott & Bond, 1973; Miller & Parry, 1974; Arnott, 1980). This argument overlooks the fact that these Fourier–Bessel structure factors continue to be significant at larger values of R, as is evident by the presence of Bragg reflections at the edges of the calculated pattern shown in Fig. 5(*a*). Only when lateral displacements of the molecules are included are the Bragg reflections truly restricted to the low-resolution region. Axial displacements that are not coupled to the rotations of the molecules remove Bragg reflections on the upper layer lines. This is illustrated in Fig. 5(*b*) for lattice distortions with $\sigma_{\text{lat}} = \sigma_{\text{axial}} = 1$ Å.

Fig. 5(*c*) shows layer-line amplitudes for small screw rotations with $\sigma_\varphi = 10°$. The pattern is similar to that for random screw disorder (Fig. 5*a*) except for some weak Bragg reflections close to the meridian on the upper layer lines and a strong meridional Bragg reflection on the 11th layer line. When lattice distortions are added to the model with small screw disorder, the diffraction pattern (Fig. 5*d*) is essentially identical to that for a random screw disorder with lattice distortions (Fig. 5*b*). The pattern is also similar to that for small rotations and lattice distortions (Fig. 4*b*) except that, in latter case, weak Bragg reflections appear on the upper layer lines.

The reason that the diffraction patterns are similar in these three cases (Figs. 4*b*, 5*b* and 5*d*) can be understood by examining the probability density functions $p(\varphi, z)$ that describe the distribution of the molecular positions. Fig. 6 shows contour plots of $p(\varphi, z)$ for (*a*) random screw disorder, (*b*) small screw rotations with $\sigma_\varphi = 10°$ and (*c*) small rotations with $\sigma_\varphi = 10°$, all in conjunction with independent axial translations with $\sigma_{\text{axial}} = 1$ Å. Although these three density functions are different,

there are considerable similarities between them. The density function for a random screw is maximum and uniform along the path $z = P\varphi/2\pi$. For small screw rotations, the probability density is maximum at the points $(\varphi, z) = (0,0)$ and $(2\pi/u, c/u)$ and decreases to about half its maximum value midway between the maxima. Otherwise, it is significant only in the region where the density for the random screw is significant. It is the helical nature of the molecule and the resulting aliasing of the distribution of molecular positions for small screw disorder that produces the similarity. Since the disorder weights, which determine the distribution of Bragg and continuous intensity on the diffraction pattern, are themselves uniquely determined by $p(\varphi, z)$, similarities in $p(\varphi, z)$ necessarily translate to similarities in the diffraction patterns. This is the source of the similarity between Figs. 5(*b*) and (*d*). The small differences in the diffraction patterns are confined to the upper layer lines and are removed if lateral disorder is present (Figs. 5*b* and *d*). Therefore, when lattice disorder is significant, it may be difficult to distinguish between the presence of small screw disorder and random screw disorder.

Overall, the probability density function for small rotations and axial translations (Fig. 6*c*) is quite similar to that for small screw rotations (Fig. 6*b*). The two density functions have maxima in the same positions although the density for small rotations and translations is not concentrated in the vicinity of the path connecting the maxima. The resulting diffraction patterns (Figs. 4*b* and 5*d*) are therefore quite similar, but there are noticeable differences.

Discrete rotations and axial shifts of the molecules can produce a wide variety of effects on the diffracted intensities, depending on the relative positions and the helix symmetry of the molecule. These effects are not confined to any particular region of a diffraction pattern. Fig. 7(*a*) shows layer-line amplitudes calculated for two equally probable positions $(\varphi_i, z_i) = (0,0)$ and $(-90°, 0)$. The effect is quite striking, with exclusively continuous diffraction near the meridian on layer lines 2 and 9. Reference to (70) shows that this is because the contribution of the Bessel orders $|n| = 2$ to the Bragg intensity on layer lines $l = 2$ and $l = 9$ is completely eliminated, while the contribution of the Bessel orders $|n| = 9$ are unaffected. Lattice disorder is not included in this calculation but, even if it were, the effects of the discrete rotation would remain evident on layer line 2. The sensitivity of the diffraction pattern to the positions of the molecules is illustrated in Fig. 7(*b*), which is calculated for $(\varphi_i, z_i) = (0,0)$ and $(30°, 0.04c)$. The upper layer lines are now dominated by continuous intensity and the disorder has little effect on the lower layer lines. This is quite different to the case shown in Fig. 7(*a*) and, in fact, is rather similar to what would be obtained for small axial shifts.

The effects of direction disorder also vary greatly depending on the location of the rotation axis relating up and down molecules. Fig. 8(*a*) shows layer-line amplitudes for direction disorder with the rotation axis at $(\varphi_0, z_0) = (165°, 0.015c)$. Comparison of this with Fig. 2 shows that the directional disorder has introduced considerable diffuse intensity into the pattern, and virtually eliminated the Bragg reflections in the region $R \simeq 0.2\,\text{Å}^{-1}$ on layer lines 2 through 4. Changing the rotation axis to $(\varphi_0, z_0) = (60°, 0.03c)$ gives the pattern

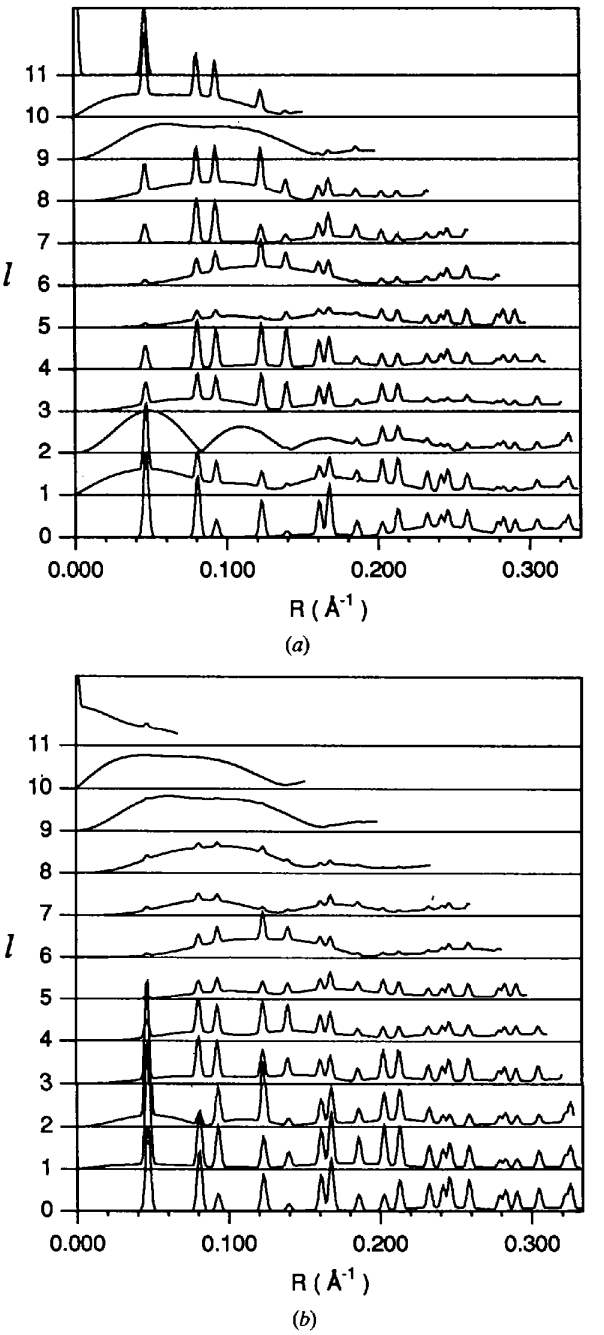

Fig. 7. Calculated layer-line amplitudes for molecules with discrete positions (*a*) $(\varphi_i, z_i) = (0,0)$ and $(270°, 0)$ and (*b*) $(\varphi_i, z_i) = (0,0)$ and $(30°, 0.04c)$.

shown in Fig. 8(*b*). This is rather similar, overall, to Fig. 8(*a*), but there are some notable differences; suppression of the Bragg reflections is greater at $R \simeq 0.05$ Å^{-1} on layer lines 1 and 2 and layer line 2 is virtually devoid of Bragg intensity.

Single quadrants of full diffraction patterns calculated for an ideal polycrystalline fiber, a fiber with random screw disorder only and a fiber with random screw disorder and lattice disorder are shown in Fig. 9. The

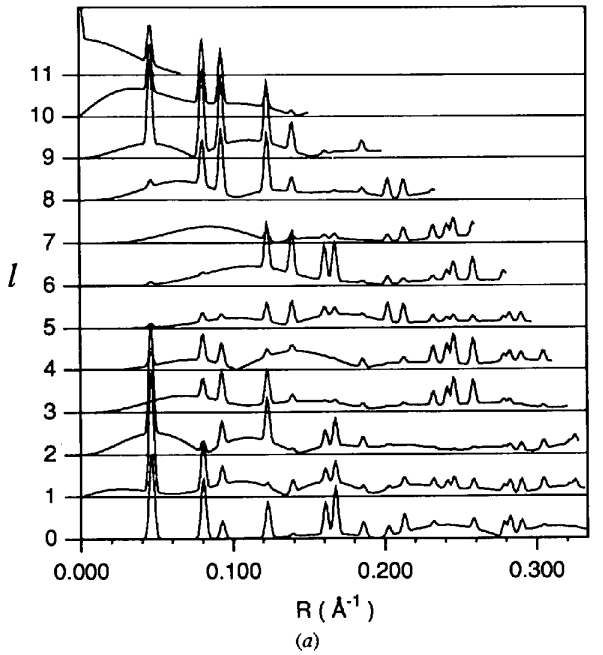

(*a*)

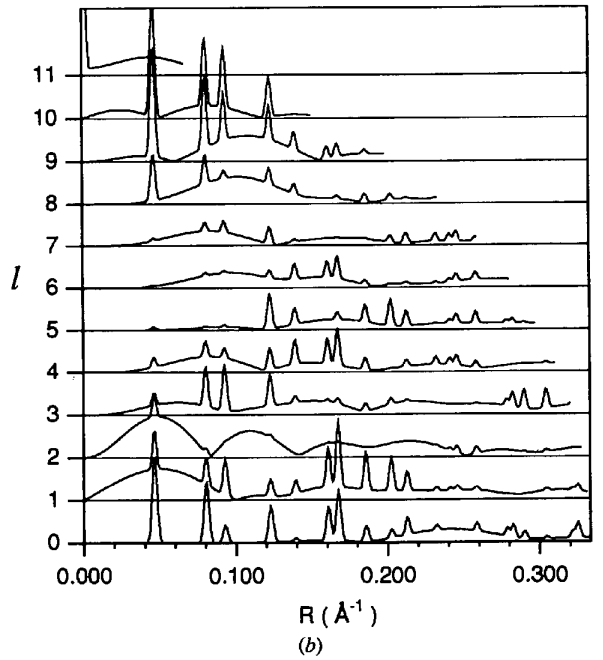

(*b*)

Fig. 8. Calculated layer-line amplitudes for direction disorder with (*a*) $(\varphi_0, z_0) = (165°, 0.015c)$, and (*b*) $(\varphi_0, z_0) = (60°, 0.03c)$.

patterns correspond to a disorientation angle $\alpha_0 = 2°$ and a coherence length $l_c = 250$ Å. The pattern for a fiber with no disorder (Fig. 9*a*) corresponds to the layer-line intensities shown in Fig. 2 and shows only Bragg reflections throughout. The patterns from screw disordered specimens (Figs. 9*b*, *c*) correspond to the layer-line intensities shown in Figs. 5(*a*) and (*b*), respectively. On each pattern, the effect of finite coherence length is most evident close to the origin, where the layer lines are smeared primarily parallel to the Z axis. Further from the origin, the spread of intensity is dominated by the angular arcing produced by disorientation. Bragg reflections appear as sharp streaks while continuous intensity appears as diffuse bands centered on the layer lines, which broaden with increasing distance from the meridian.

The effect of screw disorder in suppressing Bragg intensity on the upper lines and replacing it with continuous intensity can be seen in Fig. 9(*b*). As described above, random screw disorder by itself does not completely remove Bragg reflections from the periphery of the pattern, and sharp reflections persist to the edge of the pattern in Fig. 9(*b*). Including lattice disorder with screw disorder removes the outlying Bragg reflections (Fig. 9*c*). Also evident in Fig. 9(*c*), close to the meridian on lower layer lines, is continuous intensity introduced by lattice disorder. This intensity is absent from the diffraction pattern for a specimen with random screw disorder only (Fig. 9*b*).

5. Discussion

The theory presented here allows calculations of continuous layer-line intensities, which incorporate both Bragg and diffuse components, diffracted by disordered polycrystalline fibers. The treatment is quite general in that it includes the effects of finite crystallite size, lattice distortions and cylindrical averaging, along with more familiar disorder that we describe in terms of substitution disorder. Simulations using this theory allow the effects of the various components of disorder on diffraction patterns to be characterized rather easily and precisely. Whole diffraction patterns are readily calculated from the layer-line intensities using standard methods to account for the effects of finite coherence length and disorientation.

For diffraction patterns characterized by Bragg reflections that are restricted to the center of a diffraction pattern and continuous diffraction elsewhere, our results show that the specimen must contain significant lattice distortions, both lateral and axial shifts of the molecules. Rotational or screw disorder are not, by themselves, sufficient to produce these diffraction effects.

The effects of lattice distortions are rather easy to interpret as they suppress Bragg reflections with increasing R and Z. Rotational and screw disorders have rather different effects. In the absence of lattice disorder, Bragg

reflections due to high-order Bessel terms are suppressed by rotational disorder. Bragg reflections that are close to the meridian therefore tend to remain unaffected. On the other hand, for screw disorder (for integral helices and the pitch of the screw disorder equal to the molecular pitch), the contributions to the Bragg reflections by Bessel terms whose orders increase with layer-line number tend to remain unaffected. On the higher layer lines, then, Bragg reflections persist further from the meridian. In all cases, however, Bragg reflections persist at high resolution, as shown in the simulations, because low-order, as well as high-order, Bessel functions have significant amplitude at high resolution. Differences between rotational and screw disorder tend to be masked by the presence of lattice disorder. Diffraction patterns that contain Bragg and diffuse components throughout reciprocal space are likely to be due to the presence of discrete or directional disorder without lattice distortions.

The probability density function $p(\varphi, z)$ that describes the distribution of molecular positions is very useful in analyzing the differences or similarities between different kinds of disorder. Because of the helix symmetry of the molecule and the resulting aliasing of the distributions, different combinations of disorders can result in distributions of positions that are almost identical. They must therefore produce almost identical diffraction patterns. This is particularly useful for understanding what is sometimes an apparent lack of uniqueness; *i.e.* a par-

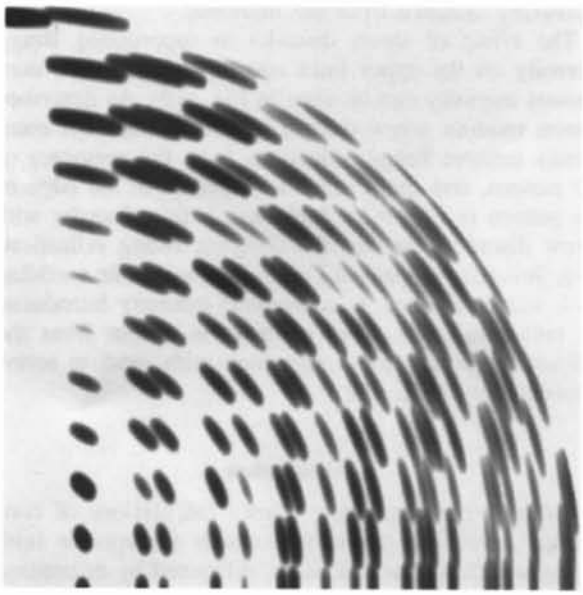

(*a*)

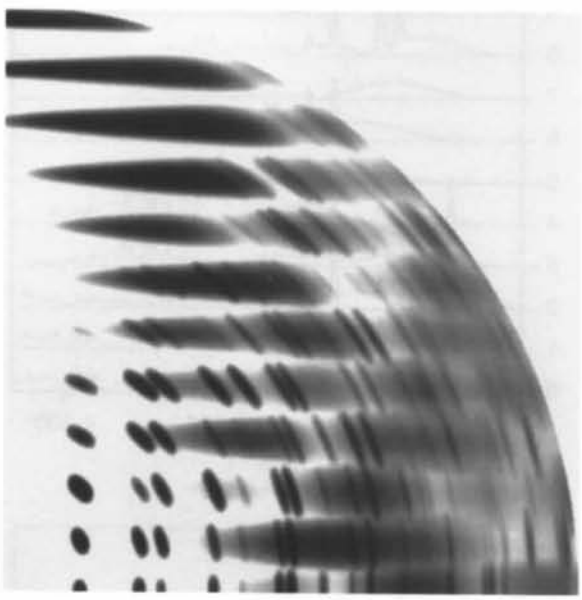

(*b*)

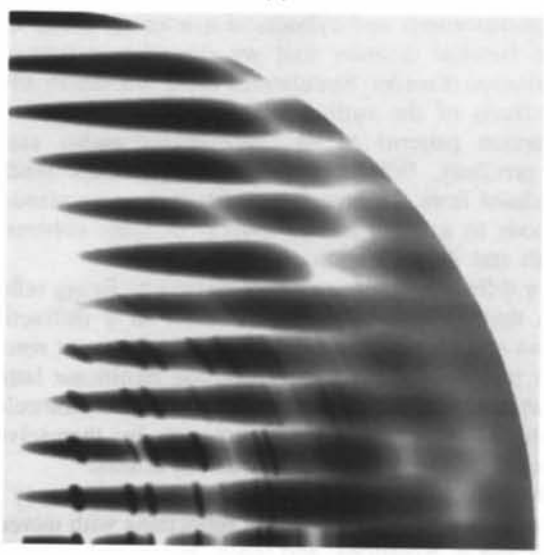

(*c*)

Fig. 9. Calculated diffraction patterns for (*a*) an ideal polycrystalline fiber, (*b*) a fiber with random screw disorder, (*c*) a fiber with random screw disorder and lattice disorder with $\sigma_{\text{lat}} = \sigma_{\text{axial}} = 1$ Å. In each case, $\sigma_0 = 2°$ and $l_c = 250$ Å.

ticular diffraction pattern being apparently interpretable in terms of different kinds of disorder. For the example shown in Fig. 6, three kinds of disorder lead to rather similar diffraction patterns because the distributions of positions of the molecules are rather similar. A more extreme, although not necessarily unrealistic, example is shown in Fig. 10 where σ_{axial} has been increased to 2 Å. The distributions of molecular positions for the three different kinds of disorder are now very similar and would lead to indistinguishable diffraction patterns. This is not because of any inherent non-uniqueness but because the different descriptions of the disorder are, in fact, almost equivalent. However, it should be pointed out that, as a result of the cylindrical averaging of the diffraction pattern, it is possible that quite different forms of disorder may lead to similar diffraction patterns.

Including the effects of disorder in the analysis of fiber diffraction patterns of this kind is important for accurate structure determination. The theory and methods presented here offer the possibility for quantifying the disorder present in particular specimens and for including the effects in structure determination. Detailed comparisons of diffraction patterns calculated using the methods described here with experimentally obtained diffraction patterns are described in a subsequent paper (Stroud & Millane, 1995*a*).

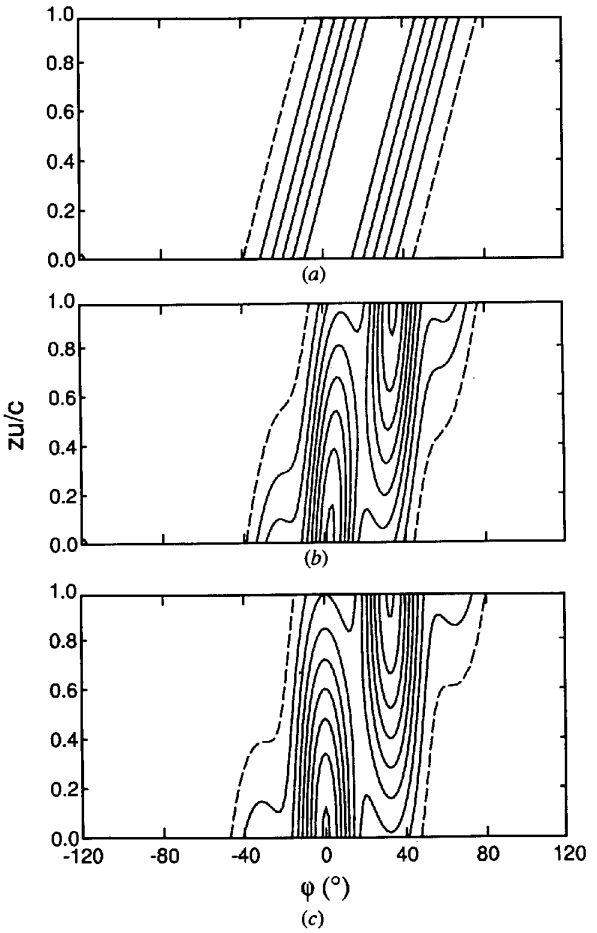

Fig. 10. Probability density functions $p(\varphi, z)$ for the molecular positions, for axial translations with $\sigma_{\text{axial}} = 2$ Å and (*a*) random screw disorder, (*b*) small screw rotations with $\sigma_\varphi = 10°$, and (*c*) small rotations with $\sigma_\varphi = 10°$. The first contour level (broken line) is at 0.05 and the increment between levels is 0.05.

There are a number of ways in which the model of diffraction by disordered fibers described here may be extended. First, the effects of disorder within molecules themselves could be incorporated. This kind of disorder has already been considered by itself (Barakat, 1987; Worthington & Elliot, 1989; Inouye, 1994) and could be included in our analysis. The effect of this would be to broaden the layer lines, modify their intensities and introduce diffuse intensity *between* the layer lines. However, distortions within the molecules are likely to be smaller and their effects on diffraction patterns less significant than the forms of disorder considered here. Second, the model described here could be extended to allow correlations between distortions at different lattice sites. Correlated lattice distortions cause Bragg reflections to broaden with increasing resolution and prevent the separation of intensity into well defined Bragg and continuous components (Welberry, 1985). A model that allows calculations of cylindrically averaged diffraction from polycrystalline fibers incorporating correlated lattice disorder is being developed (Stroud, 1993; Stroud & Millane, 1995*b*).

Supported by Purdue University and the US National Science Foundation (DMB-8916477 and MCB-9219736 to RPM).

References

ABRAMOWITZ, M. & STEGUN, I. A. (1972). *Handbook of Mathematical Functions*. New York: Dover.

ARNOTT, S. (1980). In *Fiber Diffraction Methods*, edited by A. D. FRENCH & K. H. GARDNER, pp. 1–30. *ACS Symposium Series*, Vol 141. Washington: American Chemical Society,

ARNOTT, S. & BOND, P. J. (1973). *Nature (London)*, **244**, 99–101.

ARNOTT, S., CHANDRASEKARAN, R., MILLANE, R. P. & PARK, H. (1986). *J. Mol. Biol.* **188**, 631–640.

ARNOTT, S. & DOVER, S. D. (1967). *J. Mol. Biol.* **30**, 209–212.

ARNOTT, S., DOVER, S. D. & ELLIOT, A. (1967). *J. Mol. Biol.* **30**, 201–208.

ARNOTT, S., SCOTT, W. E., REES, D. A. & MCNAB, G. C. A. (1974). *J. Mol. Biol.* **90**, 253–267.

BARAKAT, R. (1987). *Acta Cryst.* A**43**, 45–49.

CLARK, E. S. & MUUS, I. T. (1962). *Z. Kristallogr.* **117**, 108–118.

COCHRAN, W., CRICK, F. H. C. & VAND, V. (1952). *Acta Cryst.* **5**, 581–586.

COWLEY, J. M. (1968). *Acta Cryst.* A**24**, 557–563.

CROWTHER, R. A., DEROSIER, D. J. & KLUG, A. (1970). *Proc. R. Soc. London Ser. A*, **317**, 319–340.

DUNITZ, J. D., SCHOEMAKER, V. & TRUEBLOOD, K. N. (1988). *J. Phys. Chem.* **92**, 856–867.

FRANKLIN, R. E. & KLUG, A. (1955). *Acta Cryst.* **8**, 777–780.

FRASER, R. D. B. & MACRAE, T. P. (1973). *Conformations in Fibrous Proteins*. New York/London: Academic Press.

FRASER, R. D. B. & MACRAE, T. P. (1987). *J. Mol. Biol.* **193**, 115–125.

FRASER, R. D. B., MACRAE, T. P., MILLER, A. & ROWLANDS, R. J. (1976). *J. Appl. Cryst.* **9**, 81–94.

FRASER, R. D. B., MACRAE, T. P., PARRY, D. A. D. & SUZUKI, E. (1969). *Polymer*, **10**, 810–826.

FRASER, R. D. B., MACRAE, T. P. & SUZUKI, E. (1978). *J. Appl. Cryst.* **11**, 693–694.
GUINER, M. A. (1939). *Ann. Phys. (Leipzig)*, **12**, 161–237.
HENDRICKS, S. & TELLER, E. (1942). *J. Chem. Phys.* **10**, 147–167.
HOLMES, K. C. & BARRINGTON LEIGH, J. (1974). *Acta Cryst.* A**30**, 635–638.
HOSEMANN, R. & BAGCHI, S. N. (1962). *Direct Analysis of Diffraction by Matter*. Amsterdam: North-Holland.
INO, T. & MINAMI, N. (1979). *Acta Cryst.* A**35**, 163–170.
INOUYE, H. (1994). *Acta Cryst.* A**50**, 644–646.
INOUYE, H., FRASER, P. E. & KIRSCHNER, D. A. (1993). *Biophys. J.* **64**, 502–519.
KLUG, A., CRICK, F. H. C. & WYCKOFF, H. W. (1958). *Acta Cryst.* **11**, 199–212.
KLUG, A. & FRANKLIN, R. E. (1958). *Discuss. Faraday Soc.* **25**, 104–110.
MAKOWSKI, L. (1978). *J. Appl. Cryst.* **11**, 273–283.
MAKOWSKI, L. (1982). *J. Appl. Cryst.* **15**, 546–557.
MARVIN, D. A., SPENCER, M., WILKINS, M. H. F. & HAMILTON, L. D. (1961). *J. Mol. Biol.* **3**, 547–565.
MILLANE, R. P. (1988). In *Crystallographic Computing* 4: *Techniques and New Technologies*, edited by N. W. ISAACS & M. R. TAYLOR, pp. 169–186. Oxford Univ. Press.
MILLANE, R. P. & ARNOTT, S. (1985). *J. Appl. Cryst.* **18**, 419–423.
MILLANE, R. P. & ARNOTT, S. (1986). *J. Macromol. Sci. Phys.* B**24**, 193–227.
MILLANE, R. P., CHANDRASEKARAN, R., ARNOTT, S. & DEA, I. C. M. (1988). *Carbohdr. Res.* **182**, 1–17.
MILLANE, R. P. & STROUD, W. J. (1991). *Int. J. Biol. Macromol.* **13**, 202–208.
MILLER, A. & PARRY, D. A. D. (1974). *Polymer* **15**, 706–712.
NAMBA, K. & STUBBS, G. J. (1985). *Acta Cryst.* A**41**, 252–262.
OKUYAMA, K., ARNOTT, S., MOORHOUSE, R., WALKINSHAW, M., ATKINS, E. D. T. & WOLF-ULLISH, C. (1980). *Fiber Diffraction Methods*, edited by A. D. FRENCH & K. H. GARDNER, pp. 409–427. *ACS Symposium Series*, Vol 141. Washington: American Chemical Society,
PAPOULIS, A. (1984). *Probability, Random Variables, and Stochastic Processes*, 2nd ed. New York: McGraw-Hill.
PARK, H., ARNOTT, S., CHANDRASEKARAN, R., MILLANE, R. P. & CAMPAGNARI, F. (1987). *J. Mol. Biol.* **197**, 513–523.
RUTLEDGE, G. C. & SUTER, U. W. (1991). *Macromolecules*, **24**, 1921–1933.
STROUD, W. J. (1993). PhD thesis, Purdue Univ., West Lafayette IN 47907, USA.
STROUD, W. J. & MILLANE, R. P. (1995*a*). *Acta Cryst.* A**51**. In the press.
STROUD, W. J. & MILLANE, R. P. (1995*b*). *Proc. R. Soc. London Ser. A*. Submitted.
STUBBS, G. J. (1974). *Acta Cryst.* A**30**, 639–645.
TANAKA, S. & NAYA, S. (1969). *J. Phys. Soc. Jpn*, **26**, 982–993.
VAINSHTEIN, B. K. (1966). *Diffraction of X-rays by Chain Molecules*. Amsterdam: Elsevier.
WELBERRY, T. R. (1985). *Rep. Prog. Phys.* **48**, 1543–1593.
WILSON, A. J. C. (1942). *Proc. R. Soc. London Ser. A*, **180**, 277–285.
WORTHINGTON, C. R. & ELLIOT, G. F. (1989). *Acta Cryst.* A**45**, 645–654.

Acta Cryst. (1995). A**51**, 790–800

Analysis of Disorder in Biopolymer Fibers

BY W. J. STROUD AND R. P. MILLANE*

Whistler Center for Carbohydrate Research, Purdue University, West Lafayette, Indiana 47907-1160, *USA*

(*Received* 5 *September* 1994; *accepted* 15 *May* 1995)

Abstract

X-ray diffraction patterns from oriented polycrystalline fibers of some biopolymers show that the molecules are disordered within the microcrystallites. Quantifying the disorder in such specimens is a necessary step for the use of their diffraction patterns for accurate structure determination. Theory and algorithms for calculating diffraction patterns from such fibers have recently been described [Stroud & Millane (1995). *Acta Cryst.* A**51**, 000–000]. Here the application of these methods to determining the kind and degree of disorder in two polynucleotide fibers is described. The more ordered system shows random screw disorder accompanied by small lattice distortions, and the more disordered system shows larger lattice distortions and significant rotational disorder. These results show the potential of these methods for determining disorder in polycrystalline fibers; uniqueness of the solutions and implications for structure determination are discussed.

1. Introduction

The molecular and crystal structures of many of biopolymers and rod-like macromolecular assemblies have been determined by X-ray fiber diffraction analysis (Arnott, 1980; Millane, 1988). In most cases, diffraction data from *polycrystalline* specimens, which are made up of small crystallites that are randomly rotated relative to each other, have been used for structural analysis (Arnott, 1980; Millane, 1988). The diffraction patterns from these specimens are equivalent to the cylindrical projection of the pattern from a single crystal and are used to determine full crystal structures. In other cases, structure determination has used diffraction data from *non-crystalline* fibers, in which the molecules are merely oriented but not otherwise organized in the speci-

* To whom all correspondence should be addressed.

ISSN 0108-7673